INTERNATIONAL ATOMIC ENERGY AGENCY
UNITED NATIONS EDUCATIONAL, SCIENTIFIC AND CULTURAL ORGANIZATION
INTERNATIONAL CENTRE FOR THEORETICAL PHYSICS
I.C.T.P., P.O. BOX 586, 34100 TRIESTE, ITALY, CABLE: CENTRATOM TRIESTE

H4.SMR/480-17

WORKSHOP ON EARTHQUAKE SOURCES & REGIONAL LITHOSPHERIC STRUCTURES FROM SEISMIC WAVE DATA

19 - 30 November 1990

Analysis of Strong Ground Motion

P. Suhadolc

Università di Trieste
Istituto di Geodesia e Geofisica
Trieste, Italy

ANALYSIS OF STRONG GROUND MOTION

Peter Suhadolc

Istituto di Geodesia e Geofisica, Universita' di Trieste
International Center for Environmental and Marine Sciences, Miramar

Plan of lecture

1. Introduction

2. Seismic strong motion: data
   - 2.1 Acquisition
   - 2.2 Digital processing
   - 2.3 Response spectra

3. Seismic strong motion: theory
   - 3.1 Earthquake sources
   - 3.2 Earthquake spectra

4. Seismic strong motion: interpretation
   - 4.1 Main features
   - 4.2 Basic interpretation
   - 4.3 Polarization analysis

5. Seismic strong motion: modeling (case studies)
   - 5.1 Direct approach
   - 5.2 Inversion approach
   - 5.3 Modeling in laterally heterogeneous media

1. INTRODUCTION

Until not very long ago strong motion records have been the interest of engineers, while seismologists have been concerned with small amplitude displacements at great distances from the source. The first studied the strong motion from a statistical point of view and considered it a white noise modulated by a filter simulating the wave propagation. The second tried to understand the generation of ground motion as a product of the seismic source and the propagation of waves.

Recent developments in strong motion instrumentation permitted to obtain records have with a wide dynamic range, in frequency and amplitude; second they have the absolute timing. The availability of a great number of such records has stimulated the developments of the theory, not last the synthesis of seismograms. Some very well instrumented events as 1979 Imperial Valley (Archuleta, 1984), 1980 Irpinia (Bernard and Zollo, 1988) and 1985 Michoacan (Anderson et al., 1986) have provided a strong motivation for this kind of research.

The seismologists now have to explain the characteristics of strong ground motion at small distances from the source and to predict this motion at certain sites for a future earthquake with given characteristics. The interpretation of a strong motion seismogram is an inverse (or indirect) problem. Fortunately, some key parameters (fault dimensions, rock properties) can be deduced by geological and geophysical means. However, there is always the problem of uniqueness. The same record can be interpreted in different ways due to the fact that one does not know with sufficient detail neither the medium nor the fracturing process at the source, and since the parameters that define the medium and the source are arbitrarily chosen. The interpretation of old accelerograms is, moreover, limited due to the lack of absolute timing and to the fact that the first arrivals might not have triggered the instrument. For these reasons the interpretations up to the 80's were in general limited to small and intermediate magnitude events.

At least four factors are responsible for the complexity of near-source strong ground motion:

1) generation of the waves at the source (double couple or moment tensor, extended source, several subfaults; non-linear elasticity);
2) propagation of waves through the medium (dispersion, attenuation, diffraction, focusing, low-velocity layers, local heterogeneities);
3) site effects (topography, near-surface low-velocity layers with strong attenuation);
4) instrument correction.

For teleseismic events the hypothesis of linear elasticity is valid and the theory of rays can be used; the source can be approximated as a point, and the wavefronts are plane waves; one can decompose longitudinal and transverse waves. There are P, S and surface waves.

In the near field there are, on the other hand, also other kinds of waves such as stopping phases and breakout phases, the source must be treated as extended, the wavefronts are curved and there are signs of non-elastic behaviour (e.g. liquefaction).

References for Section 1

Anderson, J.G., Bodin, P., Brune, J.N., Prince, J., Singh, S.K., Quaas, R., and Onate, M., 1986. Strong ground motion from the Michoacan, Mexico, earthquake. Science, 233, 1043-1049.

Archuleta, R. J., 1984. A faulting model for the 1979 Imperial Valley earthquake. J. Geophys. Res., 89, 4559-4585.

Bernard, P. and Zollo, A., 1989. The Irpinia (Italy) 1980 earthquake: detailed analysis of a complex normal faulting, J. geophys. Res., 94, 1631-1647.

2. SEISMIC STRONG MOTION: DATA

2.1 Acquisition

Accelerographs

Accelerographs are instruments that record the acceleration of the ground as a function of time. They consist of two parts: a triaxial sensor and the recorder. They can be of two types: analogic or digital. For example,
a) Mechanical-optical-photographic (Standard in US for 50 yrs)
b) Waxed paper system (used in Japan in the past)
c) Direct digital (cassette, FD or solid-state) recording

Nowadays digital instruments are more and more deployed, since they present several advantages over analog ones.
a) A bigger dynamic range so that large and moderate accelerations can be recorded with the same instrument, with higher precision.
b) The pre-event memory, so that even if triggered by later phase arrivals, the first arrivals can be also retrieved and so the complete record of motion is available.
c) Easy processing, since no digitazation is required.

The majority of digital accelerometers have no longer the standard electromagnetic sensor. They operate as a force-balance accelerometer, which is schematically presented in Fig. 2-1.

Let the ground move with (horizontal) acceleration a, so that the mass m will move with respect to the frame, assumed rigidly connected with the ground. The relative movement detectors P_1 and P_2 sense the displacement of the mass and send a current I through the coil. The current produces a force opposite to the movement of the mass forcing it to stay at rest.

The inertial force due to the acceleration is F=ma, while the force F_I associated with the current I is $F_I = BlnI$, with B the intensity of the magnetic field due to the permanent magnet, l is the length of one loop and n is the number of loops in the coil. When the forces are at equilibrium in the frequency range where the system is linear, $F = F_I$ and one has

$$I = \frac{m}{Bln} a$$

The acceleration values can be therefore obtained from I.

Simplified analysis

A typical accelerogram will be a:
a) 35 or 70 mm film negative
b) photographic enlargement or copy on paper of a)

c) computer plot of digitized data (a computer file)
d) reproduction in book or report of the above

A copy of a typical most complete form of analog accelerogram (Fig. 2-2) will contain:
a) Time code (WWVB or simlar)
b) Three components of acceleration
c) One or two fixed traces
e) Relative time marks, generated by internal timing circuit or by external radio signal

Time code serves for positive identification of earthquake and for synchronizing various accelerographs. Fixed traces provide means for correcting for certain types of spurious motion (small transverse motions etc.) Time marks needed to read time on record, since non-uniformities in the record speed may occur. In working with copies care must be taken of possible scale changes and distortions. Good practice is to include a small scale on original.

The most important information required for interpreting traces is the transducer sensitivity, expressed as cm/g trace displacement on original film or as counts/g on digital records. The instrument manufacturer provides a calibration sensitivity for each acelerometer trace. An overall calibration can be carried in the field by the user on the complete assembly by rotation the whole accelerograph in the earth's gravitational field through a measured angle (90° tilt) and noting the corresponding trace deflections (accuracy of about 1 %).

Vertical motions have usually higher frequencies and somewhat lower amplitudes. As a rough average for past earthquakes, vertical motions are usually about two-thirds the amplitude of horizontal components.

At most stations earthquake waves emerge at near vertical angles, so the starting mechanism of the accelerograph is set to respond to vertical rather than horizontal motion. The acceleration threshold can be adjusted from 0.005 g to 0.05 g, with a flat frequency response from 1 to 10 Hz and a rapid cutoff above 10 Hz to eliminate false starts. The total time elapsing from triggering to full operating capability is not greater than 0.1 s in old analog instruments. Digitally recording accelerographs have a pre-event memory (around 5 to 10 s), which permits to record the whole signal plus some background noise.

Information which can be obtain by visual inspection of accelerogram and simple scaling is:

a) peak acceleration
b) time duration of strong shaking
c) frequency of predominant waves and rough idea of frequency range
d) amplitude and frequency relationships between vertical and horizontal motions
e) approximate distance from recording site to earthquake hypocenter (in case of small-magnitude events that produce recognizable P- and S-wave arrivals.

Pattern recognition

A collection of representative accelerograms is shown in Fig. 2-3 (Hudson, 1979). One typical horizontal component is given for each event. Many different shapes and sizes are seen, the eye being a sensitive pattern recognition instrument. Many different characteristics can be distinguished in such a way, which might be difficult to describe quantitatively through simplified representations (e.g. peak distribution statistics, frequency spectra). The similarity of a new record with an old one, for which considerable information as to damage and so forth might be available, could provide important rapid information also for decision-makers (e.g. need to evacuate a building, empty a reservoir, carry out expensive inspection procedures).

2.2 Digital processing

Accelerogram digitization or digital data provide many advantages:

a) increased resolution and higher dynamic range
b) correction for transducer
c) integration of accelerograms
d) calculation of frequency and response spectra
e) easier statistical studies and plots in any desired form or scale.

A knowledge of the limitations of the measurements and of the data processing will ensure against misinterpretation. For example, the data processing procedures impose definite high and low frequency limits on the calculated spectrum curves.

Digitization

Some digitizers are provided with an automatic stepping device, but it has been found to be better to digitize on an unequal-time basis, picking prominent points on the record, and then to convert the data to eqal-time intervals by an interpolation program.

Most accelerograms are digitized with an average of about 50 points per second and there are from 1200 to 2400 points per g, giving a resolution of at least 0.1 %. A limiting factor might be the length of the record and the trace has to be digitized in pieces (minimize the effects of fitting together the various sections!).

The fixed traces and the internal time marks are also digitized and smoothed by a weighted running average over three points. The fixed traces are then subtracted from the acceleration traces.

An overall check of the digitazation is carried out by producing a plot of the digitized data and comparing it with the original record.

Accuracy

Experiment. Digitize a straight line sloping from the lower left corner of the digitizing table to the upper right one. The size of the line was similar as to an aceleration trace. Result of different operators is shown in Fig. 2-4.

The high frequency fluctuations indicate to a very exaggerated scale the individual choices made by the operators in setting the crosshair to the center of the photographic trace image. The long period curved baseline is a consequence of an inaccuracy within the tracking mechanism of the digitazing machine.

The variations are largely random in nature, the digitizing errors closely fitting a Gaussian distribution. The mean deviation is just about one digitizer point. The digitizing interval has to be chosen so small that the noise is at a considerable higher frequency than the maximum desired signal frequency, thus making it possible to filter out these errors.

On the other hand the noise spectrum at long periods (doble integrated random digitization errors plotted versus period) shows that the limit to analysis is set at about 16 s.

The integration process is critical for long period motions since a zero baseline shift of 0.001 g can produce at 20s period a displacement error of about 2 m!

Filtering

Filtering is therefore needed to control accelerogram errors. In fact, high frequency errors make it very difficult to carry out any processes involving differentiation, while it does not disturb the integration processes. On the other hand long period errors influence very much integration processes affect little differentiation ones. The double integration of accelerograms to produce ground velocities and displacements requires a minimization of long-period errors, while transducer corrections requires the reduction of high frequency errors. It is better to limit the information to a frequency band for which a known accuracy can be attained rather than to retain additional information at higher and lower frequencies which may contain large and uncertain errors. Band -pass filtering is therefore applied.

A given running average scheme is equivalent to passing a signal through a low pass filetr with certain frequency characteristics. Unequal weights in the running average process permits a closer fit to the ideal low pass filter shape. The cosine shape time window is equivalent, for the three points, to the 1/4, 1/2, 1/4 weighting. For typical earthquake accelerograms, the averaging extends over 250 data points, weighted according to the time window function shown in Fig. 2-5. For symmetrical weighting functions there are no phase shift difficulties. The standard filter of Fig. 2-5 is called an "Ormsby" filter.

In applying running averages the beginnign and end of accelerograms are extended. To minimize distortions a reflected portion of the record is added at each end: $a(-t)=a(t)$ and $a(T+t)=a(T-t)$.

The high-pass filtering is achieved by subtracting the low pass filter signal from the original signal.

Transducer corrections

Accelerometer transducers commonly used in strong motion accelerographs have natural frequencies of about 25 Hz and damping of about 60% of critical. Such transducers give a reasonably acurate representation of ground acceleration over the frequency range 0 to 20 Hz. Above about 20 Hz the transducer response drops off with frequency (Fig. 2-6).

The only parameters appearing in the transducer equation are the natural frequency of the system ω_n and the fraction of critical damping ζ. Test switches on the accelerograph provide for testing ω_n and ζ.

Transducer corrections are introduced as follows (Caltech processing):

1) start with uncorrected accelerogram digitized at unequal time intervals;
2) interpolate equally spaced time data to facilitate digital filtering;
3) extend accelerogram at beginning and end to permit running averaging;
4) low-pass filter to remove high-frequency noise
5) reduce number of points by decimation to reduce computer time;
6) calculate derivatives of the time series;
7) substitute in transducer equation to find true ground acceleration.

Double integration of records

1) Least square fit acceleration;
2) extend record for filtering;
3) low pass filter with equal weight running average (pre-filter reduces computer time);
4) decimate data (reduce computer time);
5) low pass filter by unequal weight running average;
6) interpolate points at same time ordinates as input accelerogram and subtract from input to produce high-pass filtered accelerogram, thus performling baseline adjustment;
7) eliminate linear trends again by least squares fit, to produce final corrected accelerogram;
8) integrate accelerogram, eliminate linear trends and low-pass filter to produce final corrected ground velocity;
9) integrate again and low-pass filter to produce final corrected ground displacements.

An example of the above procedure is shown in Fig. 2-7. An extensive discussion of the analog to digital conversion of accelerograms and, in general, on acquisition and processing strong ground motion is given in Basili (1987).

2.3 Response spectra

A more exact description of the frequency content of the earthquake ground motion requires some kind of frequency spectrum curve, as response spectrum or Fourier amplitude spectrum.

Response spectra, calculated from the recorded ground acceleration, are plots of the maximum response to the earthquake of a simple oscillator over a range of values of its natural period and damping. They were first obtained by Biot (1941), while the following calculation scheme for computing them is due to Nigam and Jennings (1969).

The equation of motion of an oscillator is

$$\ddot{x} + 2\beta\omega\dot{x} + \omega^2 x = -a(t)$$

in which b is the fraction of critical damping, w is the natural frequency of vibration of the oscillator. Assuming that a(t) can be approximated by a segmentally linear function, the above equation can be written as

$$\ddot{x} + 2\beta\omega\dot{x} + \omega^2 x = -a_i - \frac{\Delta a_i}{\Delta t_i}(t - t_i)$$

with $\Delta a_i = a_{i+1} - a_i$, and $\Delta t_i = t_{i+1} - t_i$. The analytical solution solution of this equation can be put in the form:

$$\begin{Bmatrix} x_{i+1} \\ \dot{x}_{i+1} \end{Bmatrix} = [A]\begin{Bmatrix} x_i \\ \dot{x}_i \end{Bmatrix} + [B]\begin{Bmatrix} a_i \\ a_{i+1} \end{Bmatrix}$$

where the matrices [A] and [B] depend only on β, ω and Δt.

The absolute acceleration of the mass at time t_i is given by

$$\ddot{z}_i = \ddot{x}_i + a_i = -(2\beta\omega\dot{x}_i + \omega^2 x_i)$$

Since β and ω are constant during the calculation of each spectrum value, and if Δt_i is constant also, the displacement, velocity and absolute acceleration at time Δt_i can be evaluated by the execution of only ten multiplication operations for each step of integration. The matrices A and B, defined by rather complicated expressions (Nigam and Jennings, 1969) need to be evaluated only at the beginning of each spectrum calculation.

To construct the response spectra, it is necessary to find the maximum values of the displacement, velocity and acceleration during a given excitation. Thus, the response spectra are given by

$$S_d(\omega, \beta) = \max_{i=1,N} [x_i(\omega, \beta)]$$

$$S_v(\omega, \beta) = \max_{i=1,N} [\dot{x}_i(\omega, \beta)]$$

$$S_a(\omega, \beta) = \max_{i=1,N} [\ddot{z}_i(\omega, \beta)]$$

in which S_d, S_v, S_a are the spectral values of displacement, velocity and acceleration, respectively, for selected values of damping and natural frequency; N is the total number of discrete points at which the response is obtained.

This process of obtaining the maximum response is approximate, since the response is found only at discrete points, whereas the true maxima may occur between such points. However estimates of the upper bound of such error show taht it is less than 1.2% if the interval of integration $\Delta\tau \leq T/20$ with T the natural period.

From S_d the pseudovelocity spectrum PSV and pseudoacceleration spectrum PSA are easily computed as follows:

$$PS_v = \omega\, S_d = (2\pi/T)\, S_d$$

$$PS_a = \omega^2\, S_d = (2\pi/T)^2\, S_d$$

A common form of the response spectrum is the so-called tripartite or four-way logarithmic plot from which the displacement, pseudovelocity and pseudoacceleration spectra can be simultaneously read (Fig. 2-8).

Notice that the Fourier spectrum can never be larger than the undamped velocity response spectrum!

Various energy expressions are also sometimes defined in such a way that they can be conveniently related to response spectra. The maximum strain energy W_s stored in the spring of the simple oscillator is:

$$W_s = (1/2)\, k\, [\, x(t)\,]^2_{max} = (1/2)\, k\, (\, S_d\,)^2$$

Writing this as energy per unit mass, E_s :

$$E_s = (k/2m)\, (\, S_d\,)^2 = (1/2)\, (\, \omega\, S_d\,)^2 = (1/2)\, (PS_v)^2$$

The square root of the total energy of the system can also be shown to be proportional to the Fourier amplitude spectrum of the ground acceleration.

References for Section 2

Basili, M., 1987. Data acquisition and processing in strong motion seismology. In: Strong Ground Motion Seismology, M. O. Erdik and M. N. Toksoz (eds.), pp. 251-331, Reidel, Dordrecht.

Biot, M. A., 1941. A mechanical analyzer for the prediction of earthquake stresses. Bull. Seism. Soc. Am., 31, 151-171.

Hudson, D. E., 1979. Reading and interpreting strong motion accelerograms. Earthquake Engineering research Institute, Berkely.

Nigam, N. C. and Jennings, P. C., 1969. Calculation of response spectra from strong-motion earthquake records. Bull. Seism. Soc. Am., 59, 909-922.

3. SEISMIC STRONG MOTION: THEORY

3.1 Earthquake sources

In order to explain observed strong ground motion one must have a realistic theory of the seismic source.

The seismic source extends over a fault plane in the Earth's interior and ruptures in a series of dislocations starting at nucleation points and propagating with different velocities. The dislocation front changes velocity in passing through asperities and barriers. The slip in each dislocation is like an elastic rebound, producing seismic waves near the front of the dislocation due to the relaxation of elastic deformation energy. The source is like a radio antenna, when the receiver is near a finite antenna the signal is complicated due to interferences produced by the finite dimensions of the antenna.

The first explanation of the earthquake process has been given by Reid with his elastic rebound theory. The movement of the rebound, however, can proceed also in an irregular manner due to friction. Irregular movements along the fault are due to stress or strength variations (asperities and barriers). The radiation is, therefore, coherent only on small portions of the fault (subfaults). This means that different faults have different radiation patterns and, therefore, the form of the related waves is different. Moreover, moving sources give rise to the Doppler effect.

The first method, the simplest mathematical model to treat the source, is the kinematic one: one has to know "a priori" the slip with time on the fault and a certain number of parameters is required for this description. Then one needs a Green's function to compute displacements at a station.

The second method makes use of differential equations of motion and includes the forces that produce the fracture. The basic model is the fracture of a crack which starts in a pre-stressed medium and then causes stress concentrations at its tips. There is a big unresolved problem associated with this method, that is the interaction between the rate of growth of the crack, the rupturing criterion and the concentration of stresses. In actual computations one uses simple homogeneous structures and numerical methods (finite differences or elements).

A third method of studying the source is due to Backus (1977a, b) in which the processes at the source are not specified, but described in terms of moment tensors of increasing order. For near-source studies higher order terms are very complicated and difficult to evaluate.

The kinematic model of the source is still the most widely used to interpret strong ground motion. Its main parameters describing the rupturing on a fault are the lenght of the fault, L, its width, W, the average slip on the fault, D, the average rupture velocity, Vr, the time of fracture of each fault element, T, and the distribution of asperity or barrier density, F(x).

The principal problem of today's theoretical seimology is to determine which of these parameters are essential, which group of parameters is optimal and how these can be evaluated from the seismograms both in the near and far field.

Today it is possible to compute synthetic seismograms for realistic models of the seismic source. However, not all the peaks observed in records can be modelled and the reciprocity theorem states that lateral heterogeneities have the same effect on waveforms as point-sources, so that not all the peaks are related to source processes. Moreover,there is the problem of uniqueness of the obtained solution.

One way of computing synthetics and explaining strong ground motion is to use a deterministic method (Bolt, 1987). The problem is that not always the short-period data in the far field agree with the high frequencies in the near field. Below about 2 Hz or above it things are not always explained in the same way: deterministic information is available only for long wavelengths, while stochastic methods are used to treat shorter ones.

A second way is to use numerical solutions: finite differences or finite elements. Some examples of these techniques will be discussed later.

3.2 Earthquake spectra

The spectra of the majority of earthquakes are much simpler than one might think and correspond very well to the extremely simple model proposed by Brune (1970). The radiation of the earthquake (dislocation, double couple) for P waves in the far field can be written as

$$u^P = \frac{1}{4\pi\rho_0\alpha_0^3}\sqrt{\frac{\rho_\theta\alpha_\theta}{\rho_\theta\alpha_\theta J}}\cdot R^P(\gamma)\cdot\dot{M}(t-T_\alpha)$$

with ρ and α the density and velocity of P waves, respectively; J is the geometrical divergence, R the radiation pattern and $\dot{M}$ the derivative of the seismic moment. A similar expression holds for S waves. The displacement produced by the source is, therefore, proportional to the derivative of the seismic moment M.

By taking the Fourier transform of the above equation one can see that that $u^P(\omega)$ is proportional to the spectrum of $\dot{M}$, or

$$\dot{M}(\omega) = \Omega(\omega) = i\omega\, M(\omega)$$

The absolute value $|\,\Omega(\omega)\,|$ of this transformation is called *earthquake source spectrum*. Its most common form is given in Fig. 3-1a, called Brune's model or ω^2 model. At low frequencies it has a constant part directly proportional to $M_0=M(\omega\rightarrow 0)$, the scalar seismic moment. At high frequency the spectrum decays inversely proportional to ω^2 . The two asymptotes cross at a frequency called *corner frequency* . It is controlled by the dimensions of the fault: for low frequencies the source appears as point-like and the waves do not notice it is finite, while for high frequencies the wavelength is smaller than the dimensions of the fault and the waves are strongly diffracted at fault boundaries. The corner frequency with dimensions T^{-1} is inversely proportional to the source duration or the source dimension, L. It is given (Brune, 1970; Madariaga, 1976) by

$$\omega_0 = 2\pi f_0 = N\beta/L$$

with N around 2.3.

To get the acceleration spectra in the far field it is enough to multiply the dislacement spectrum by ω^2. The acceleration spectrum (Fig. 3-1b) has a

"plateau" between the corner frequency and a frequency called f_{max} (Hanks, 1982).

This plateau is called band limited white noise and corresponds to the Fourier transform of a stochastic signal with f_{max} as the correlation frequency. Signals shorter than $t_{min} = (f_{max})^{-1}$ are strongly correlated, longer ones are independent. In the far field the correlation is due to the strong attenuation of the body waves passing through the upper mantle. At low frequencies the spectrum is controlled by the rupturing duration, as seen. Such a spectrum corresponds in general to a series of impulses of duration t_{min} distributed in a window of duration f_0^{-1}.

To observe such spectra the station must correctly record frequencies lower than the corner frequency and higher than the cutoff frequency. For teleseismic events f_{max} is around 1 Hz for P and 0.25 Hz for S waves.

Between 30° and 100° the attenuation is practically independent of the distance, meaning that the attenuation in the lower mantle is negligible with respect to that in the asthenosphere.

Brune's spectrum has to be modified, and we can write the acceleration radiation in the far field as:

$$u^P(\omega) = \frac{1}{4\pi\rho_0\alpha_0^3} \cdot \sqrt{\frac{\rho_0\alpha_0}{\rho_s\alpha_s}} \cdot R^P(\gamma) \cdot M_0 \cdot S(\omega, \omega_0) \cdot F_Q(\omega, t^*)$$

with

$$S(\omega, \omega_0) = \frac{\omega^2}{1 + (\omega / \omega_0)^2}$$

the acceleration spectrum at the source as defined by Brune (1970) and

$$F_Q = \exp(-\omega t^*)$$

$$t^* = \int \frac{dt}{2Q}$$

where the integral is along the source-receiver path.

Of course this representation is the average of many events, but a single event might deviate considerably from this (e.g. Mexico 1985 event).

Note that Brune's spectrum does not say anything about the phase spectrum. Madariaga (1977) has shown that Brune's spectrum is a universal property of all fault models based on fracture mechanics. A propagating crack produces a strong concentration of stresses near the crack tip, which appears as a linear source of high-frequency radiation. In fact, the radiation is emitted when the crack velocity changes abruptly (barriers giving rise to stopping phases, asperities giving rise to acceleration phases). A realistic model for the origin of high frequencies is therefore a series of stochastic impulses of more or less short duration distrubuted in a period of time of the order of the rupturing duration. The association of these impulses to the complexities of the rupturing is one of the most fascinating field of present-day seismology.

Near the source the accelerations are larger and richer in high frequencies. For distances lesser than 100 km the waves propagate completely in the lithosphere. Studying spectra of strong ground motion at these distances, it has been seen that the Brune's model is valid, at least in first approximation, also in these cases. The difference is that the cutoff frequency f_{max} is situated beyond about 6 Hz.

Analyzing seismograms recorded near the source in Friuli (De Natale et al., 1987) it has been seen that these appear to be similar to those recorded on short-period instruments at teleseismic distances. The signal appears as a sequence of successive impulses released in a time window related to the duration of rupturing at the source. Is this complexity related to the source or to the structure? Since signals related to small magnitude events contain in general only one short-duration peak, the complexity is mainly due to source effects.

As anticipated the spectra have the shape predicted by Brune's model, only the scaling is different. The cutoff frequency is around 8 Hz, the corner one around 1 Hz. The presence of frequencies higher than for teleseismic signals is explained by the fact that the lithosphere is less dissipative.

This similarity with the teleseismic case can be explained considering that the theory of wave propagation (with its assumptions of rays...) is essentialy valid (few modifications by Spudich and Frazer, 1984 and Bernard and Madariaga, 1984) also at small distances from the source, as long as the source-receiver distance remains smaller than the wavelength.

The origin of the cutoff frequency f_{max} is still debated. Some authors (Aki, 1984) think that it is produced by a characteristic dimension of the source. Others (e.g. Hanks, 1982; Anderson and Hough, 1984) think it is due to the attenuation of waves. Is the source that does not radiate frequencies higher than about 6 Hz or is the attenuation of superficial layers that filters them effectively out? Observations show that f_{max} is almost independent of magnitude and path of propagation and that it is stable in time.

Aki (1984) argues that a minimum rupturing length, of the order of a couple of hundred meters, is necessary to accelerate the rupture sufficiently to produce radiation of seismic waves and that f_{max} is related to this characteristic length.

Anderson and Hough (1984), on the other hand, show that the decay of frequencies higher than f_{max} is exponential and can be written as $\exp(-\kappa\omega)$ with

$$\kappa \approx 2\pi/f_{max}$$

This decaying can be easily related to the attenuation in the upper layers of the crust:

$$\kappa = t^* = \int \frac{dt}{Q}$$

As already discussed, some spectra do not behave as Brune's and present peaks at certain frequencies or a slow transition to the plateau. Some authors (Papageorgiou and Aki, 1984; Gusev, 1984) proposed more complicated models to explain these features.

One possible spectrum shows an ω^{-1} envelope before the plateau (Fig. 3-2). The intermediate frequency is called f_{patch} by Papageorgiou and Aki (1983) and

reflects the existence of coherent zones with lengths proportional to $(f_{patch})^{-1}$. f_{patch} is probably inversely proportional to the mean radius of the active subfaults which radiate on the surface of the fault (Fig. 3-3). See also Boatwright (1984) for details.

References for Section 3

Aki, K., 1984. Asperities, barriers, characteristic earthquakes and strong ground motion prediction. J. Geophys. Res., 89, 5867-5872.

Anderson, J. N., and Hough, S.E., 1984. A model for the shape of the Fourier amplitude spectrum of acceleration at high frequencies. Bull. Seism. Soc. Am., 74, 1969-1993.

Backus, G.E., 1977a. Interpreting the seismic glut moment of total degree two or less. Geophys. J. R. Astr. Soc., 51, 1-25.

Backus, G.E., 1977b. Seismic sources with observable glut moment of spatial degree two. Geophys. J. R. Astr. Soc., 51, 27-45.

Bernard, P., and Madariaga, R., 1984. A new asymptotic method for the modeling of near-field accelerograms. Bull. Seism. Soc. Am., 74, 539-559.

Boatwright, J., 1984. The effect of rupture complexity on estimates of earthquake source size. J. Geophys. Res., 89, 1132-1146.

Bolt, B. A. (ed.), 1987. Seismic Strong Motion Synthetics, Academic Press, Orlando.

Brune, J. N., 1970. Tectonic stress and the spectra of seismic shear waves from earthquakes. J. Geophys. Res., 75, 4997-5009.

De Natale, G., Madariaga, R., Scarpa, R., and Zollo, A., 1987. Source parameter analysis from strong motion records of the Friuli, Italy, earthquake sequence (1976-1977). Bull. Seism. Soc. Am., 77, 1127-1146.

Gusev, A. A., 1983. Descriptive statistical model of the earthquake source radiation and its application to an estimation of short-period strong motion. Geophys. J. R. Astr. Soc., 74, 787-808.

Hanks, T. C., 1982. f_{max}. Bull. Seism. Soc. Am., 72, 1867-1880.

Madariaga, R., 1976. Dynamics of an expanding circular fault. Bull. Seism. Soc. Am., 66, 639-666.

Madariaga, R., 1977. High frequency radiation from crack (stress drop) models of earthquake faulting. Geophys. J. R. Astr. Soc., 51, 625-651.

Papageorgiou, A. S., and Aki, K., 1983. A specific barrier model for the quantitative description of inhomogeneous faulting and the prediction of strong ground motion, I, Descritpion of the model. Bull. Seism. Soc. Am., 68, 693-722.

Spudich, P., and Frazer, L. N., 1984. Use of ray theory to calculate high-frequency radiation from earthquake sources having spatially variable rupture velocity and stress drop. Bull. Seism. Soc. Am., 74, 2061-2082.

4. SEISMIC STRONG MOTION: INTERPRETATION

4.1 Main features of strong ground motion

For a long time the key parameter describing strong ground motion has been the peak ground amplitude (acceleration, velocity, displacement). This developed in the '60 due to the limited amount of available records. Initially only PGA was considered, the maximum observed values being of the order of 0.3 to 0.5 g.

In the 70' it soon became clear that the information PGA was giving is limited and that PGA is not a stable parameter. Records with peaks much greater than those usually observed have been obtained (e.g. Imperial valley 1979: 1.7 g in vertical, 1.2 g in horizontal components). It was recognized that these PGA are due to few peaks not representative of the whole record. Most important: it was observed that high PGA have been recorded near relatively small events (Bear Valley 1972, M_L 4.7 and Ancona 1972, M_L 4.5 had 0.6 g). A given PGA may correspond to strong ground motions much different in seismic energy and spectrum. For high frequencies it may vary around 10% without changing significantly the spectral curves of total energy. PGA might not coincide temporally on the horizontal components and are not the result of any vectorial composition. Moreover, in almost all the cases these correspond to very high frequencies. For this reason one started to consider also PGV and PGD.

Due to its widespread use, PGA has been correlated to a number of parameters, first of all local magnitude. The quantity of seismic energy released in a certain frequency band around the fault is a function of the rock properties around the dislocation more than a result of the energy released on the whole fault plane. A limiting value seems to exist for the energy released and therefore for PGA. At Tabas, Iran, 1968 M_L 7.7 event 10 km from the fault a value of 0.8 g has been observed. Therefore, we can conclude that high-frequency PGA near the fault are approximately the same for large and moderate events.

The decay of PGA with distance, still a key relationship in earthquake engineering and seismic risk studies even if subject to large uncertainties, has been treated mainly with empirical laws (e.g. Campbell, 1981; Joyner and Boore, 1981). A theoretical explanation in terms of structure and source parameters has been advanced by Suhadolc and Chiaruttini (1987).

The duration of the earthquake depends mostly on the fault dimensions. However, strong deviations from the mean that are due to source multiplicity, medium stratification and site effects, are quite common.

Can groups of arrivals (as P, S or surface waves) be recognized in strong motion records in the near field? Accelerograms consist of lots of high-frequency peaks and considerable variability in amplitudes. However, strong motion records can sometimes roughly be divided into three parts: an increasing amplitude part of principally P waves; a central part with high amplitudes reaching more or less two lines parallel to the base line; a final amplitude decreasing part (coda). The first part is composed basically of P waves, then depending on the distance

from the fault (parts) there will be a mixture of P and S waves coming from different parts of the fault. Later, especially in the horizontal components, surface waves appear, in generally mixed with S waves. Some impulses can be explained also as free surface rupture (having about 1 s duration impulse).

The remaining part (mainly higher frequencies) must be ascribed both to an unknown distribution of asperity and barrier density along the fault as well as to lateral heterogeneity and site effects. In general one can suppose that each important fault has its own characteristic distribution of asperities and barriers.

The effect of horizontal layering is well known. Near the fault lateral heterogeneities might be strong. Sedimentary basins have been studied (e.g. Bard and Bouchon, 1980a; 1980b; Campillo and Bouchon, 1985; Fäh, et al., 1990), but of difficult treatment (finite differences, analytical approaches with simplicistic and non-realistic assumptions...) due to mode conversions, diffraction, dispersion and resonances. Elementary approaches (ray theory) might, on the other hand, give misleading answers!

Seismic waves are also laterally refracted, due low-velocity material around the fault (fault gouge). This might also imply that in viscoelastic media the separation into P and S waves might not occur. Moreover anisotropy (e.g. Zollo and Bernard, 1989) and strong attenuation (Q factor as low as 10 or 20) might play an important role.

The problem is that the structure is in most cases unknown. Therefore, most strong variations in intensity of ground motion is commonly attributed to the above causes.

4.2 Basic interpretation

Vectorial decomposition of three components of motion

When three components of motion are available. Vertical component in general different from horizontal ones. First contains P and SV waves plus higher modes of Rayleigh waves, second has SH waves. For small, possibly also moderate, events one can rotate horizontal components into longitudinal and trasverse ones; for large events in the near field this concept looses significance.

In presence of low-velocity layers near surface most of the motion can be vertical, therefore vertical component might be dominant.

Possible, when rotation feasable, to compute the particle motion in the horizontal or a vertical plane.

Velocity and displacement

By integration (attention!) one can work with nine components. The integration process filters out most of the high-frequency stochastic components of motion. For this reason the interpretation of phases is simpler for velocities; also the comparison with theoretical seismograms is easier, since most theoretical models give best results for frequencies lower than 1 Hz.

Transformation of accelerograms into seismograms due to known instrumental responses.

Kanamori and Jennings (1978) have estimated M_L from accelerograms by feeding the records into the response of a Wood Anderson instrument. This facilitates also the interpretation of the groups of arrivals.

Source mechanism

Theoretical computations show that fault mechanism influences strong ground motion considerably (e.g. Suhadolc and Chiaruttini, 1987). However few available records that permit to make analysis. Most records are due to complex fracturing.

Doppler effect

Directivity or focusing effect, verified in the far field (see Ben-Menahem and Singh, 1972) have not been sufficiently clarified in the near field. The factor

$$F = [1 - (v/\beta)\cos\theta]^{-1}$$

with θ the angle between the direction of wave propagation and trajectory of source movement. Might give an effect as big as factor of 10.

Interaction between records and theoretical modelling

It is important to know some information about the nature of the seismic source, its distance and its dimensions. In this way using appropriate velocities of P and S waves one can find ranges of values for the ir arrivals at different stations and the duration of the record. Since no arrival of phases tables are available for strong ground motion, it is useful to have theoretical records for different parameters (depth, focal mechanism, distance...) in order to compare them with observations.

Arrays of strong motion instruments

Of big help in the interpretaton are arrays of accelerometers, especially when digital and with a common (absolute) timing. E.g. linear array across the Imperial Valley fault (1979 event), SMART-1 array in Taiwan.

Wavefronts propagating across the array (their direction and apparent velocity) can be determined with a crosscorrelation of arrival times of peaks and troughs at each station. An alternative way to identify the predominant energy is to make an f-k (frequency-wavenumber) analysis (e.g. Abrahamson and Darragh, 1987).

4.3 S-wave polarizations

Source and propagation effects are responsible for the complexity of near source seismic waveforms, rendering them difficult to interpret. Usually the three components of ground motion are analysed, but wave-motion may be also parametrized by its modulus and direction (the polarization unit vector).

For near-source records it seems (Bernard and Zollo, 1989; Zollo and Bernard, 1989) that for a given medium there exists a specific distance and frequency range where the polarization in the S window is not significantly perturbed by the velocity structure and can be used for constraining the earthquake mechanism and location of point-like sources.

The acceleration ground motion can be expressed as

$$\mathbf{a} = S\mathbf{A}\mathbf{s} = |a|\,\mathbf{p}$$

with S a scalar function at the source, **A** a matrix depending on the radiation pattern, **s** the unit slip vector, $|a|$ the modulus of the considered ground motion time function and **p** the polarization unit vector. **p** does not change in direction, but changes sign with time and is a function of the mechanism only, while $|a|$ is a function of both mechanism and amplitude. In fact, polarization is expected not to be significantly perturbed by near-surface site effects, anelastic attenuation, or geometrical divergence, which, on the other hand, strongly affect amplitudes. When the amplitude and mechanism are both poorly constrained, it seems more suitable to invert first for the mechanism with polarization data and then for the source amplitude, rather than to simultaneously analyze the three components of **a**.

Booth and Crampin (1985) indicate that the polarization analysis has to be restricted to incidence angles below the critical one and to frequencies between 1 and 10 Hz, so that the polarization appears to be stable in time (small elliptical particle motion). In the case of real data the main difficulty is to know whether or not a given station receives the S phase at a subcritical incidence. A simple criterion appears to be the importance of the vertical motion of the S arrival for post-critical angles Booth and Crampin (1985), and of strong ellipticity for near-critical ones (Bernard and Zollo, 1989).

A low-velocity upper layer will enlarge the source-station distance range where the free surface effects are easy to deal with, due to sub-critical arrivals, but may generate strong multiples and converted phases, whose incoherent arivals makes the polarization variable (Fig. 4-1).

Bernard and Zollo (1989) have investigated the approximation of using ray theory synthetics for polarization studies. In general, shallow sources (less than about 3 km) give a very variable polarization for distances grater than 5 km abd cannot be modeled with ray theory. They have shown that variability in the polarization increases with distance and seismic wave frequency, because of the simultaneously increasing number of relevant reflectors, refractors and scatterers. These phenomena severly degrade the 1 to 2 Hz polarization for distances greater than 50 km.

Polarization may be also modified by anisotropy. Zollo and Bernard (1989) have shown that the observed waveform complexity of the October 15, 1979, 23:19 Imperial Valley aftershock was due to a delayed S-arrival time on two orthogonal components, with the fast S-wave mainly polarized in the N-S direction. After the polarization correction the retrieved source mechanism is much simpler (Fig. 4-2).

Such studies point out the need to perform polarization analysis of strong-motion near-source records before applying any inversion procedure to 3-component ground motion amplitude data.

References to Section 4

Abrahamson, N.A., and Darragh, R.B., 1987. Origin of scattered waves recorded by the SMART-1 strong motion array (abstract). Seism. Res. Lett., 58, 15.

Ben-Menahem, A., and Singh, S. J., 1972. Computation of models of elastic dislocations in the earth. In: Methods of Computational Physics, vol. 12, B. A. Bolt (ed.), Academic Press, New York.

Bernard, P., and Zollo, A., 1989. Inversion of near-source S polarization for parameters of double-couple point sources. Bull. Seism. Soc. Am., 79, 1779-1809.

Booth, D. C., and Crampin, S., 1985. Shear wave polarizations on a curved wavefront at an isotropic free surface. Geophys. J. R. Astr. Soc., 83, 31-45.

Bard, P.Y. and Bouchon, M., 1980a. The seismic response of sediment-filled valleys. Part I. The case of incident SH waves: Bull. Seism. Soc. Am., 70, 1263-1286.

Bard, P.Y. and Bouchon, M., 1980b. The seismic response of sediment-filled valleys. Part II. The case of incident P and SV waves. Bull. Seism. Soc. Am., 70, 1921-1941.

Campillo, M. and M. Bouchon, 1985. Synthetic SH seismograms in laterally varying medium by the discrete wavenumber method. Geophys. J. R. astr. Soc., 83, 307-317.

Campbell, K. W., 1981. Near-source attenuation of peak horizontal acceleration. Bull. Seism. Soc. Am., 71, 2039-2070.

Fäh, D., Suhadolc, P. and Panza, G.F., 1990. Estimation of strong ground motion in laterally heterogeneous media: modal summation - finite difference approach. Proc. 9th European Conference on Earthquake Engineering, Kucherenko Tsniisk USSR Gosstroy, Moscow, 4A, 110-120.

Joyner, W. B., and Boore, D. M., 1981. Peak horizontal acceleration and velocity from strong-motion records including records from the 1979 Imperial Valley, California, earthquake. Bull. Seism. Soc. Am., 71, 2011-2038.

Kanamori, H., and Jennings, P. C., 1978. Determination of local magnitude M_L from strong-motion accelerograms. Bull. Seism. Soc. Am., 68, 471-485.

Suhadolc, P., and Chiaruttini, C., 1987. A theoretical study on the dependence of the peak ground acceleration on source and structure parameters. In: M. O. Erdik and M. O. Toksoz (eds.), Strong Ground Motion Seismology, Reidel, Dordrecht, 143-183.

Zollo, A., and Bernard, P., 1989. S-wave polarization inversion of the 15 October 1979, 23:19 Imperial Valley aftershock: evidence for anisotropy and a simple source mechanism. Geophys. Res. Lett., 16, 1047-1050.

5. SEISMIC STRONG MOTION: MODELING

To infer the nature of the earthquake source from observations of seismic ground motion has always been one of the main tasks of seismology. Although much effort has gone into calculationg Green's functions and modeling earthquake rupture at teleseismic distances (e.g. Nabelek, 1984; Dziewonski and Woodhouse, 1985), such observations are limited by interference of waves propagationg from different parts of the fault. The effect of this interference on source modeling is that the short-scale length details of the rupture history of an earthquake can not be recovered.

To resolve the seismic source in grater detail it is therefore necessary to use data from the near-source region. However, two main difficulties arise: the lack of accurate Green's functions and the unavailability of sufficient near-source seismic data.

A wide range of complete Green's functions technique are now available (see e.g. Bolt, 1987). All techniques, except those using empirical Green's functions (Hartzell, 1978), calculate either exact Green's functions in idealized Earth models, or calculate approximate Green's functions in more realistic Earth models. In either case, one is faced with the task of matching an inadequate, incomplete data set with an imperfect forward model of the effects of faulting on the radiated elastic field.

In such situations it is essential to use prior information (e.g. geodetic observations, extent of aftershock zone, location of hypocenter, etc.) to constrain the infinite number of possible models. Another class of constraints is the requirement tnat the solution be as simple as possible, which amounts to minimizing a norm that defines some measure of solutions complexity.

The first works dealing with the modeling of near-source ground motion were those of Aki (1968) and Trifunac (1974). In the last ten years several papers have appeared dealing with the inverse problem for source parameters on a finite fault.

The extensive data set generated by the 1979 Imperial Valley earthquake resulted in some interesting papers. Olson and Apsel (1982) presented a model in which rupture occurred on 20 subfaults allowed to slip more than once. In this formulation the problem was linear since the rupture times were specified a priori. A similar technique has been used by Hartzell and Heaton (1983), who considered 56 subfaults and limited the variation of rupture velocity. Archuleta (1984) derived a more detailed model of rupture by trial and error modeling of velocity waveforms; in his model with subfaults slipping only once, he found that amplitude changes resulted in small predictable effects on waveforms, while changes in time of rupture resulted in large unpredictable effects.

Takeo (1987) presented a linearized inversion for fault rupture parametrizd by variable slip and rupture time applied to the 1984 Naganoken-Seibu earthquake. He also specified the rupture propagation within each subfault. Beroza and Spudich (1988) performed a linarized inversion for slip intensity and rupture time of the 1984 Morgan Hill, California, earthquake strong-motion data. They solved the inverse problem for the model perturbation using a tomographic back projection technique (Olson, 1987), while asymptotic ray theory was used to calculate theoretical seismograms.

In the following two applications of strong ground motion interpretation to the 1980 Irpinia, Italy, earthquake will be presented. The first (Vaccari et al., 1990) is a direct trial and error method to fit the envelope and frequency content of strong ground motion records for frequencies up to 10 Hz. The second (Harabaglia et al., 1988; Suhadolc et al., 1990) is an inversion of strong ground motion data for slip amplitude on the fault for frequencies up to 1 Hz.

5.1 Direct approach

It is well known that a very complicated source model was responsible of the large Irpinia, 1980 earthquake. So, even if the event was well monitored by the strong ground motion recordings (Berardi, Berenzi and Capozza, 1981), it is not an easy task to retrieve the source model from the available data. In the following, we discuss the results of a trial-and-error procedure which makes use of the deterministic computation of synthetic signals at high frequencies. A rough fit of the accelerometric data is obtained, both in the time and in the frequency domain, for the six stations closest to the epicentral area. The recorded accelerograms are shown in Fig. 5-1.

The purpose of the adopted trial-and-error procedure is to select, among a quite wide distribution of possible solutions, the one which can explain the main features of the accelerometric data with a low number of point sources. At first, 13 evenly spaced locations have been selected along the fault; subsequently three more have been added near the Brienza station (see Fig. 5-2). The spacing of these locations, hereafter called epicentres, is 5.7 km. A total of 10 hypocentral depths between 2 and 17.5 km have been considered for each epicentre, and the corresponding theoretical accelerations have been computed, by the modal summation technique (Panza, 1985; Panza and Suhadolc, 1987), at the six stations under consideration. The structural model used to construct the synthetics is derived from the "Model A" proposed by Del Pezzo et al. (1983), and have been kept constant for all the stations. A time delay and a relative weight have been subsequently assigned to each point source, in order to simulate with a time sequence the evolution and size of the rupturing process.

To be kept in the global source model, a point source has to satisfy the following conditions:

1) Its relative time delay, measured from the nucleation time of the fracture (first point source of the sequence), together with the distance and time shift from the nearest point source, must be compatible with a sub-shear rupture velocity. There are no exceptions to this rule.

2) The amplitudes measured at the six stations, after assigning a weight to the point source, must be in agreement with the observed ones. Since the local site effects are not taken into account in the computation of the synthetic accelerograms, some tolerance is allowed for this rule.

The synthetic signals of Fig. 5-3 are the final result of the trial-and-error procedure. In their analysis, some caution is necessary in the interpretation of the obtained sequence of point sources, since the representation theorem states that also the effect of lateral variations can be represented by point sources. In any case, we consider it quite remarkable that even neglecting lateral variations, the synthetic signals of Fig. 5-3 have been obtained superimposing the effect of only 12 point sources, chosen accordingly to the above mentioned conditions. A vertical section of the retrieved source model is given in Fig. 5-4, while the temporal evolution of the rupturing process is shown in Fig. 5-5. Each point source can be considered to represent a breaking asperity (Kanamory and Stewart, 1978), but the interpretation in terms of the barrier model (Das and Aki, 1977; Aki, 1979) is equally possible.

Since the aim in our modelling is not a peak-to-peak matching, but rather an envelope fit, a check on the quality of the result can be given by the comparison

of the amplitude spectra of the observed and synthetic records. Vaccari et al. (1990) showed that even by considering a few point sources with relatively simple time functions, the synthetic spectra have the tendency to reproduce the general features of the observed ones.

Even if the source model is intended to be only a rough estimate aimed at identifying the areas where a major slip occurred, it seems possible to outline the overall initial rupturing process as propagating bilaterally, with a sub-sonic velocity, possibly along the path schematized by the dotted line in Fig. 5-4. The distribution of point sources simulating the propagation upwards and to the NW from the nucleation point seems to be quite regular both in space and time. This part of the fracturing process can be, therefore, assumed to be almost continuous.

The southeastern branch of the fracture, on the other hand, is not so well linked in space and time with the central fracture process and could be assumed to represent an almost "independent" event. The later parts of the strong motion records are reproduced by means of some shallow point sources, with varying seismic moment, simulating the stopping of the rupture below or within the upper sedimentary cover and, very likely, some effect of the lateral heterogeneities.

The waveform fitting can be obviously improved considering a large number of point sources but, at present, we consider that a close waveform matching at frequencies higher than a few Hz is not relevant for the understanding of the source process. To be able to use high-frequency information in a deterministic way it is, in fact, necessary to better understand the high-frequency behaviour of earthquake rupturing and to know and consequently to model the lateral variations of the structural parameters to the scale of the involved wavelengths.

5.2 Inverse approach

Realistic deterministic models of the seismic ground motion for frequencies lesser than about 1 Hz can be obtained, provided a few conditions are met: a sufficiently dense local network of (preferably digital and with absolute time) strong motion instruments that have recorded the event and the capability to compute complete synthetic seismograms. The first condition is quite well approximated for the Irpinia, Italy, November 23, 1980 earthquake; the second is achieved through the mode summation technique. After obtaining through a simple minimization process a source model that reproduces the observed recordings, one can also use it to obtain estimates of the seismic ground motion at those places, where the earthquake has not been recorded.

The inverse method applied to the same data set as in Section 5.1, Gaussian filtered with the cutoff frequency set at 1 Hz, iterates through a series of "loops". In the "outer loop" we define the spatial location of each fault, we discretize it as a dense grid of point sources and assign an average slip direction. For each point source, we compute the synthetic accelerogram realtive to all the network sites, assuming a normalized moment of 1 dyne-cm. The actual computation is performed through a modal summation technique (Panza, 1985; Panza and Suhadolc, 1987). The i-th synthetic record can be expressed as

$$s_i(t) = \Sigma_j m_j a_{ij}(t-t_j) \qquad (5\text{-}1)$$

where a_{ij} is the synthetic accelerogram at the j-th point source, m_j is the seismic moment and t_j is the time delay from the nucleation time. Such a problem is highly non-linear. Attempts to linearize (5-1) fail since derivatives with respect to time and derivatives with respect to moment are non homogeneous quantities and their relative weight is unknown. To solve the problem in the least square sense, we had to damp the time perturbations, requiring the time shift to be smaller than the dominant period of the signal. Under these assumptions, the invesion for the rupture time becomes meaningless since the difference between starting and final model will be negligible.

We therefore decided to introduce a new "loop", fixing the time parameters and defining different models with variuos rupture velocities expressed as percentage of the S-wave velocity. Then for each of these models we can solve a much simpler linear problem in the form of

$$\mathbf{Am = d}$$

applying the conjugate gradient technique (Press et al., 1986). In this way we can evaluate several different models and choose the "best" ones following several criteria. Models that do not reproduce certain phases are preferred to models that produce extra ones. This is because our simplified earth model cannot acount for later arrivals, diffractions, etc. Normally we do not put any constraint on the parameters, but models with more than 5% of negative seismic moment were discarded. We also normalize the records according to their maximum amplitude. This is equivalent to weight a record in proportion to its duration. We do so because a short and compact signal generally means that the source is nearby and our algorithm is valid only in the far field approximation (Panza and Suhadolc, 1987).

We have evaluated several hundred models differing by fault location, slip direction, and time history and we have also conducted tests against synthetic data. On the basis of this experience, we beleive that the fault strike does not vary by more than 3° in either direction for a long fault and 8° for a short one. We cannot say the same for dip and slip direction: the first can yield uncertainties of up to 30° and the latter up to 60°. Nevertheless, we have seen taht we can normally recover the location of the center of mass of an asperity within about 3 km and a couple of seconds, even for Earth models with S-wave velocities differing by as much as 0.5 km/s. Whenever there is a misparametrization, the inversion will lead to a defocusing of the model and an eventual enlargement of the asperities. For this reason we have greater confidence in the location of the asperities and to a certain extent in their size but we do not beleive in their predicted shape. Finally, there is another effect that counteracts the previous one: whenever there are two asperities with same epicentral location and different depth, the shallower one will mask the effect of the deeper one, as long as the shallower asperity has a moment at least 0.1 times that of the deeper. It is a well known fact that a fault normally nucleates at the bottom and that the rupture is usually unilateral (King, 1986). Unfortunately this means that as the rupture progresses and reaches the surface, we can only see shallow features and we loose the possibility to study the behaviour of the fault at depth. Therefore, although most of our models do not show any significant energy release at depth, there is no reason to beleive that this is true. It just means that the resolving power of accelerograms is not sufficient, or in other words, that the solutions involving the features of the deeper part of the fault are in the nullspace of **A**. We want, however, to emphasize that accelerogram data are able to single out those features that are primarily responsible for the destructive ground motion.

In our inversion we use the six ENEA stations closest to the fault, namely Auletta, Bagnoli, Bisaccia, Brienza, Calitri and Sturno. The structural model is the same as in Section 4.4.1 (Fig. 5-6). There is still some disagreement between variuos authors on the number of faults involved (Westaway and Jackson, 1987; Bernard and Zollo, 1989; Pantosti and Valensise, 1990): our model has four faults - the synthetic accelerograms resulting from it are shown in Fig. 5-7).

There is little disagreement on the nucleation site and the strike of the main fault. Following Vaccari et al. (1990), we place the nucleation point at 40° 49' 45" N and 15° 17' 30" E (depth of 12 km), slightly to the north of Westaway and Jackson (1987). The strike angle is 320° and the dip angle is 70° towards the northeast. Since the slip direction is not easily resolvable, we fixed it to 270° for all the faults. Along the main fault we can locate four major asperities (A1 to A4 in Fig. 5-8). The first three can be easily associated with surface faulting seen by Pantosti and Valensise (1990) and with the model proposed by Westaway and Jackson (1987). The last asperity, A4 is placed near Sturno. Unfortunately Sturno is the only record where this asperity is relevant, so we cannot really say if it actually happened on a bending of the main fault as claimed by Bernard and Zollo (1989) or along a continuation of the main fault. Since the record shows a strong impulsive signal we suppose it must have been a short shallow subevent whose wavetrains were quickly scattered and attenuated. The total moment release along the main fault is about 8 x 10^{25} dyne-cm with an average slip of about 50 cm. The maximum slip along the main asperities is more than 3 m, a rather high value but not too far away from that predicted by theoretical models (King, 1986) in case of surface displacements of about 1 m as observed by Pantosti and Valensise (1990).

The second main subevent, the so-called "20 s" subevent probably took place along two different faults. It started along a subhorizontal fault to the southeast of the main fault, as proposed by Bernard and Zollo (1989), and then propagated upward along the continuation of the main fault to the south. In our model the subhorizontal plane has a dip of 20° but we think that this parameter is not well constrained. The nucleation point is at 40° 43' 00" N and 15° 30' 00" E with nucleation time of 15.6 s. The subhorizontal plane is not strictly necessary to explain the main phases at the two southernmost stations Auletta and Brienza, but is the only way to generate a signal of length comparable to that observed on the two records. It also helps to reproduce the long-period arrivals at Brienza. The presence of the asperities A5, A6 and A7 is a constant in all the models with a subhorizontal fault, as is the lack of radiation release between A5 and A7. We think that this is a real feature since no other asperity could mask this effect. The seismic moment of the subhorizontal fault is about 1.5 x 10^{25} dyne-cm and that of the subvertical fault is about 2.5 x 10^{25} dyne-cm. The average slip on these faults is 30 cm and 60 cm, respectively. As far Auletta is concerned, the station was clearly on a radiation minimum with respect to the main event, as pointed out by Vaccari et al. (1990), but to match its later phases with those of the "40 s" subevent, we need a trigger time of 22 s, a value much higher than that commonly accepted by other authors.

The last subevent the so-called "40 s" subevent is far the less resolvable. We tried to invert for models with nucleation points corresponding to those proposed by Bernard and Zollo (1989), as well as at a couple of other locations. The only acceptable location seems to be taht of their model A (40° 52' 00" N, 15° 21' 00" E). The time shift is 41 s, higher than usually accepted and the nucleation depth is only 8 km. The fault has a strike of 95° and a dip of 75° toward north. The strike is the only well resolved parameter. The total moment release is too high compared to the dimensions of the fault (4 x 10 dyne-cm, average slip 60 cm), the nucleation point is not at the bottom as should be expected and, finally, the actual distribution of moment along the fault is not realistic, since all the small asperities are spaced in time exactly 1 s one from the other. The most probable explanation is that the structural model we used does not describe adequately the area around the 40 s fault.

5.2.1 Estimates of strong ground motion in absence of records

If we take alternatively away one record from the data set used in the inversion procedure and we perform the minimization again, we end up with the models shown in Fig. 5-9. In the same figures both the observed and the theoretical signals relative to the record not used in each minimization are also shown. These theoretical signals have been estimated on the basis of the source model, obtained not taking into account that station.

The accord between observed and estimated records at the stations of Bagnoli, Bisaccia and Calitri is by far better than that at the other three stations. If we compare the varius source models obtained using the different data sets, it can be seen that those obtained discarding, in turn, the records of Auletta, Brienza and Sturno show no trace of the source that in each case brought the main contribution to the related records. The accelerograms that are estimated for these sites are mainly derived from the uniform slip distribution all over the nearby portions of the fault, which is basically untouched by the minimization process. The records of Bagnoli, Bisaccia and Calitri are, on the other hand, mainly affected by the same subevents, namely those occurring in the first 7 s. Withdrawing from the inversion of one of these recordings is not crucial. Reliable estimates of the strong ground motion is therefore possible only in areas in the middle of the array covered by a sufficiently dense number of stations, otherwise the ability to realistically estimate the strong ground motion at sites between the stations will be severly hampered.

This procedure allows one to retrieve the main features of the source model and to estimate sufficiently well the ground motion at sites where it has not been recorded. From the example described above, the length of the accelerograms, the dominant phases and the maximum amplitudes are in close accord with the experimental ones, with the notable exception of the first arrivals at Bisaccia, where also the maximum amplitude is smaller than the observed one. It is also possible to estimate the main accelerograms features due to the 40-s subevent, although the source model can be questionable to some extent, due to the poor resolution of the available data with respect to this subevent.

Since a certain tradeoff is expected between the rupturing velocity, the location of the main sources of energy release and the structural model, the obtained source model is a gross approximation of the real one. However, since it permits to get realistic estimates of the recorded signals and it is basically in accord with the simpler models proposed by other authors, it can be considered a sufficiently good and realistic approximation, at least for practical engineering purposes.

An improvement of the source model can be obtained considering more stations and the horizontal components of motion. This in turn, requires the use of at least 2-D models to take into account different tectonic settings and site effect. This can be done through the combined use of the modal summation and finite differences methods (see below), but, at present, we lack a reliable picture of the structural model of the Irpinia earthquake area to warrant this attempt.

5.3 Modeling in laterally heterogeneous media

The influence of local soil conditions and topography on earthquake ground motion is very important in the estimation of seismic hazard and in the design of high-risk constructions in seismically active regions. Besides the well-known increment in amplitudes of incident waves due to low impedances in sediments, and the mechanical resonances of the sedimentary layers in the vertical direction (Haskell, 1962), focussing of wave energy can occur above structures with irregular interfaces (Campillo et al., 1989). This effect is limited to the observation points just above the irregularities and can induce a large level of differential motion, so that close observation points show different amplitudes and signal durations. On the other hand, horizontal interfaces, as transitions from bedrock to sediments, can induce local surface waves in the sedimentary layers (Bard and Bouchon, 1980a; 1980b). They can well dominate the signal, especially close to the transition zone. Subsurface soil formations with mechanical impedances lower than that of the overlaying material can trap energy. This energy can be scattered to the surface at lateral heterogeneities. Theoretical studies have shown the important influence of lateral irregularities on strong ground motion (Sanchez-Sesma, 1988) and can help in the interpretation or prediction of seismic patterns. Many methods have been proposed to estimate the influence of lateral heterogeneities on strong ground motion, but most of them suffer from the use of nonrealistic wavefields (e.g.Bard and Bouchon, 1980a; 1980b; Campillo and Bouchon, 1985; Bard and Gariel, 1986; Zahradnik and Hron, 1987; Sanchez-Sesma et al., 1987).

To overcome this drawback a hybrid approach to this problem has been developed, combining modal summation and the finite difference method (Fäh et al., 1990). The method allows to take into consideration source, path and local soil effects in the computation of the wavefield induced by a seismic event. The propagation of waves from the source up to the local laterally heterogeneous medium can be suitably handled by the modal summation method for a layered model (Panza, 1985; Panza and Suhadolc, 1987; Florsch et al., 1990), while in the laterally heterogeneous medium the 2-D finite difference method (Korn and Stöckl, 1982; Virieux, 1986) is applied.

5.3.1 Method

The model is divided into two regions, the 1-D layered structure and the region containing the 2-D heterogeneities (Fig.5-10). The source is located in the laterally homogeneous part. For a double-couple seismic source Ben-Menahem and Harkrider's formalism (1964) is used, with the convention for the orientation given by (Panza et al., 1973). Time duration is available assuming a convolutive model (Ben-Menahem, 1961). For the calculation of ground motion at the surface of the heterogeneous region, the computations are separated into two parts. The propagation of the waves from the source up to two vertical adjacent grid lines (Fig.5-10) is computed with the modal summation method (Panza, 1985; Panza and Suhadolc, 1987). The resulting time series are then used as input in the region where the finite difference method is applied. In the SH computations the displacements are used as input, whereas in the P-SV case the input consists of the velocity time series. Following (Alterman and Karal, 1968), the algorithm is designed in such a way that the vertical grid lines, where the wavefield is introduced, are transparent for any reflections emanating from the heterogeneous part of the model.

To provide a more realistic modelling, anelastic behaviour has been included in the calculations. Emmerich and Korn (1987) proposed a method to incorporate attenuation into numerical time-domain computations of SH-wave propagation. This approach is based on the rheological model of the generalized Maxwell body and allows to approximate the viscoelastic modulus by a low-order rational function of frequency. By choosing the rheological model of the generalized Maxwell body, the viscoelastic modulus M can be written in the frequency domain as:

$$M(\omega) = M_R + \sum_{j=1}^{n} a_j \cdot \delta M \cdot \frac{i\omega}{i\omega + \omega_j} \qquad (1)$$

Each part of the sum represents a classical Maxwell body with viscosity $a_j \cdot dM/w_j$ and elastic modulus $a_j \cdot dM$ (Christensen, 1982). The term M_R represents an additional elastic element. The coefficients of the viscoelastic modulus are determined by fitting a certain Q-law in a limited frequency band. Substitution of all elastic moduli by viscoelastic moduli of the form (1) and transformation of the stress-strain relation in the time domain ends up in a formulation which can be handled with a finite difference algorithm (Emmerich and Korn, 1987; Faeh, 1990).

5.3.2 Examples of computation

Local soil conditions and subsurface topography can significantly affect the characteristics of ground motion during an earthquake. This is clearly seen in the first example where a simple model is shown. It consists of a layered structure with only three layers over a halfspace and an alluvial valley (Fig.5-11).

In Fig.5-12 computations for SH and P-SV wave propagation are presented. A right-lateral strike-slip point source is placed on a vertical plane at 1.5 km depth. The strike-receiver angle has been chosen in the direction of the maximum of the radiation pattern, which for SH-waves is in the strike direction and for P-SV waves forms an angle of 45° with the strike direction. The upper frequency limit is set to 1 Hz. At a distance of 39 km from the source (first receiver: R1) the ground displacement is formed almost entirely by the first few modes. The P-SV waves are more dispersed than the SH ones, due to the slow fundamental Rayleigh wave. The amplitudes of SH waves are about four times larger than the ones of P-SV waves.

In the alluvial valley, the signals undergo significant changes, both in duration and amplitudes (Fig. 5-12). There is a large amplitude increment of the signals inside the basin. This is due to the impedance in the basin, which is lower than in the surrounding structure. The dispersion is stronger inside the valley than outside, because of the stronger vertical velocity gradient in the basin. This leads to a longer duration of ground motion in and behind the basin. The effect of the right edge of the valley is small, so almost no reflections occur. A great part of the energy from the incident modes is transferred to other modes, especially to the fundamental mode. In the valley the differential motion observed at nearby receivers is very big in the high-frequency part of the signals. This is due to conversions of surface waves into body waves.

The second example of computation is a more realistic one, treating theoretically the local effects of the May 6, 1976 Friuli Earthquake in the Friuli Plane. On the basis of the available information (Barbano et al., 1985; Mao and Suhadolc, 1987) a structural model is given for the Friuli central region near Udine (Fig. 5-13). The main features of the N-S cross-section are a series of overthrusts in the southern part and two quarternary basins. The layered model includes two low-velocity zones (Mao and Suhadolc, 1987; 1990). It corresponds to the structure at the left boundary of the laterally heterogenous model.

A simulation of the May 6, 1976, Friuli earthquake (point source approximation with the source parameters taken from Suhadolc et al. (1988)) is given in Fig. 5-14. Only SH-wave propagation is considered. The accelerations at an array of observation points are presented for the layered structure and the laterally heterogeneous structure. The upper frequency limit is 5 Hz. The existence of the low-velocity zones implies the propagation of considerable amounts of energy even at depths, where the low-velocity zones are located. Due to the limitation of the finite difference grid in depth, the waves propagating below this limit can not be introduced in the finite difference computations. As the distance from the vertical grid lines, where the wavefield is introduced in the model, to the right artificial boundary is less than twice the depth of the finite difference model, the seismograms are complete for all rays having an angle of incidence with respect to the vertical direction bigger than 60°.

In the part where sediments are absent, the signals have no high-frequency content and the amplitudes are smaller than elsewhere. An increase in the amplitude and in the duration of the signals is observed at the edges of the two alluvial basins. In the second basin, after the outcrop, local surface waves are formed which are dominating the signals. They are trapped in the uppermost layer. As Q is 20 in this layer, the local surface waves are damped very rapidly. The computation for the layered model can be used to control the reflections from the artificial boundaries. They can be absorbed completely.

Combining the mode summation method with the finite difference technique makes it possible to study local effects even at large distances (hundreds of kilometers) from the source. Such an approach can be applied in microzonation studies and provides realistic estimations of the ground motion for two-dimensional anelastic models. The method can account for source, path and local effects. The dominant components of ground motion and the frequency content of the signals depend on the source depth, orientation and the rupture process. Anelasticity, trapping of energy in low-velocity zones and the geometrical spreading are the main factors influencing the propagation of seismic waves over large distances. They can be accounted for by a layered anelastic model. Heterogeneities with size comparable to the wavelength of the incident wavefield can generate significant spatial variations of the ground motion. The closer they are to the observation point the more important are the effects. They can be studied with the 2-D finite difference method. As shown in the examples, the main effects are an increment in amplitudes and durations of the signals inside sedimentary basins, the redistribution of energy between different modes at lateral heterogenities, the exitation of local surface waves at transition zones between bedrock and sediments and a large differential motion for nearby points close to the transition zone.

References to Section 5

Aki, K., 1979. Characterization of barriers on an earthquake fault, J. geophys. Res., 84, 6140-6148.

Aki, K., 1968. Seismic displacements near a fault. J. Geophys. Res., 73, 5359-5376.

Alterman, Z.S., and Karal, F.C., 1968. Propagation of elastic waves in layered media by finite difference methods. Bull. Seism. Soc. Am., 58, 367-398.

Archuleta, R. J., 1984. A faulting model for the 1979 Imperial Valley earthquake. J. Geophys. Res., 89, 4559-4585.

Barbano, M.S, Kind, R. and Zonno, G., 1985. Focal parameters of some Friuli earthquakes (1976-1979) using complete theoretical seismograms. J. Geophysics, 58, 175-182.

Bard, P.Y. and Bouchon, M., 1980a. The seismic response of sediment-filled valleys. Part I. The case of incident SH waves: Bull. Seism. Soc. Am., 70, 1263-1286.

Bard, P.Y. and Bouchon, M., 1980b. The seismic response of sediment-filled valleys. Part II. The case of incident P and SV waves. Bull. Seism. Soc. Am., 70, 1921-1941.

Bard, P.Y. and Gariel, J.-C., 1986. The seismic response of two-dimensional sedimentary deposits with large vertical velocity gradients. Bull. Seism. Soc. Am., 76, 346-366.

Ben-Menahem, A., 1961. Radiation of seismic surface waves from finite moving sources, Bull. Seism. Soc. Am., 51, 401-435.

Berardi, R, Berenzi, A. and Capozza, F., 1981. Campania-Lucania earthquake on 23 November 1980: accelerometric recordings of the main quake and relating processing, in Contributo alla caratterizzazione della sismicità italiana, pp. 1-103, ENEA-ENEL, Rome.

Bernard, P. and Zollo, A., 1989. The Irpinia (Italy) 1980 earthquake: detailed analysis of a complex normal faulting, J. geophys. Res., 94, 1631-1647.

Beroza, G. C. and Spudich, P., 1988. Linearized inversion for faumlt rupture behavior: application to the 1984 Morgan Hill, California, earthquake. J. Geophys. Res., 93, 6275-6296.

Bolt, B. A., 1987. Seismic strong motion synthetics. Academic press, Orlando.

Campillo, M. and M. Bouchon, 1985. Synthetic SH seismograms in laterally varying medium by the discrete wavenumber method. Geophys. J. R. astr. Soc., 83, 307-317.

Campillo, M., Sanchez-Sesma, F. J. and Aki, K., 1989 Influence of small lateral variations of a soft surficial layer on seismic ground motion. J. Soil Dyn. Earthquake Eng. (in press).

Christensen, R. M., 1982. Theory of viscoelasticity. Academic Press.

Das, S. and Aki, K., 1977. Fault planes with barriers: A versatile earthquake model, J. geophys. Res., 82, 5658-5670.

Del Pezzo, E., Iannaccone, G., Martini, M. and Scarpa, R., 1983. The 23 November 1980 southern Italy earthquake, Bull. seism. Soc. Am., 73, 187-200.

Dziewonski, A. M. and Woodhouse, J. H., 1985. Studies of the seismic source using normal-mode theory. In: Earthquakes: observation, theory and interpretation, North Holland, Amsterdam.

Emmerich, H. and Korn, M., 1987. Incorporation of attenuation into time-domain computations of seismic wave fields. Geophysics, 52, 1252-1264.

Fäh, D., 1990. Influence of local soil condition and subsurface topography on strong ground motion. PhD thesis, in preparation.
Fäh, D., Suhadolc, P. and Panza, G.F., 1990. Estimation of strong ground motion in laterally heterogeneous media: modal summation - finite difference approach. Proc. 9-th European Earthquake Engineering Conference, Moscow, 4B, 110-119.
Florsch, N., Fäh, D., Suhadolc, P. and Panza, G.F., 1990. Complete synthetic seismograms for high-frequency multimode Love waves. In preparation.
Harabaglia, P., Suhadolc, P. e Panza, G.F., 1987. Il terremoto irpino del 23.11.1980: meccanismi di rottura dall'inversione di dati accelerometrici. Atti 6° Convegno Gruppo Nazionale di Geofisica della Terra Solida, CNR, Roma, 119-124.
Hartzell, S. H., 1978. Earthquake aftershocks as Green's functions. Geophys. Res. Lett., 5, 1-4.
Hartzell, S. H. and Heaton, T. H., 1983. Inversion of strong ground motion and teleseismic waveform data for the fault rupture history of the 1979 Imperial Valley, California earthquake. Bull. Seism. Soc. Am., 73, 1553-1583.
Haskell, N.A., 1962. Crustal reflection of plane P and SV waves. J.Geophys.Res. 67, 4751-4767.
Kanamori, H. and Stewart, G., 1978. Seismological aspects of the Guatemala earthquake of February 4, 1976, J. geophys. Res., 83, 3427-3434.
King, G., 1986. Speculations on the geometry and termination processes of earthquake rupture and its relation to morphology and geological structure. PAGEOPH, 124, 567-585.
Korn, M. and H. Stöckl, 1982. Reflection and transmission of Love channel waves at coal seam discontinuities computed with a finite difference method. J.Geophys., 50, 171-176.
Mao, W.-J. and Suhadolc, P., 1987. L'area sismica del Friuli: inversione dei tempi di arrivo per un modello di velocita' e modellazione di forme d' onda accelerometriche. Atti 6. Convegno Gruppo Nazionale di Geofisica della Terra Solida, CNR, Roma, 451-459.
Mao, W.J. and Suhadolc, P., 1990. Ray-tracing, inversion of travel times and waveform modelling of strong motion data: application to the Friuli seismic area NE Italy. Submitted to Geophys. J. Int.
Nabelek, J. L., 1984. Determination of earthquake source parameters from inversion of body waves. Ph.D. thesis, Mass. Inst. of Technology, Cambridge.
Olson, A. H., 1987. A Chebyshev condition for accelerating convergence of iterative tomographic methods - solving large lest-squares problems. Phys. Earth Planet. Inter., 47, 333-345.
Olson, A. H. and Apsel, R. J., 1982. Finite faults and inverse theory with applications to the 1979 Imperial Valley earthquake. Bull. Seism. Soc. Am., 72, 1969-2001.
Pantosti, D., and Valensise, G., 1990. Faulting mechanism and complexity of the 23 November 1990, Campania-Lucania earthquake, inferred from surface observations. J. Geophys. Res., 95, 15319-15341.
Panza, G.F., 1985. Synthetic seismograms: The Rayleigh waves modal summation. J. Geophysics, 58, 125-145.
Panza, G.F., Schwab, F.A. and L. Knopoff, 1973. Multimode surface waves for selected focal mechanisms, I. Dip-slip sources on a vertical fault plane. Geophys. J. R. Astr. Soc., 34, 265-278.
Panza, G.F. and Suhadolc, P., 1987. Complete strong motion synthetics, in Seismic Strong Motion Synthetics, Computational Techniques, (B.A. Bolt, Editor), Academic Press, Orlando, vol. 4, pp. 153-204.

Press, W., Flannery, B., Teukolsky, S. and Vetterling, W., 1986. Numerical recipes. Cambridge University Press, Cambridge.
Sanchez-Sesma, F.J., 1988. On the seismic response of alluvial valleys. In: J. Bonnin et al. (eds.), Seismic Hazard in Mediterranean Regions, 85-104.
Sanchez-Sesma, F.J., Chavez-Garcia F.J. and M.A. Bravo, 1987. Seismic response of a class of alluvial valleys for incident SH waves. Bull. Seism. Soc. Am., 78, 83-95.
Suhadolc, P., Cernobori, L., Pazzi, G. and Panza, G.F., 1988. Synthetic isoseismals : applications to Italian earthquakes. In J. Bonnin et al. (eds.), Seismic Hazard in Mediterranean Regions, Kluwer, Dordrecht, 205-228.
Suhadolc, P., Harabaglia, P. and Panza, G.F., 1990. Deterministic modeling and estimate of strong ground motion: the Irpinia, Italy, November 23, 1980 earthquake. Proc. 9th European Conference on Earthquake Engineering, Kucherenko Tsniisk USSR Gosstroy, Moscow, 4A, 110-120.
Takeo, M., 1987. An inversion method to analyze the rupture process of earthquakes using near-field seismograms. Bull. Seism. Soc. Am., 77, 490-513.
Trifunac, M. D., 1974. A three-dimensional dislocation model for the San Fernando, California, earthquake of February 9, 1971. Bull. Seism. Soc. Am., 64, 149-172.
Vaccari, F., Suhadolc, P. and Panza, G.F., 1989. Irpinia, Italy, 1980 earthquake: waveform modelling of strong motion data, Geophys. J. Int., 101, 631-647.
Virieux, J., 1986. P-SV wave propagation in heterogeneous media: velocity-stress finite-difference method. Geophysics, Vol. 51, 889-901.
Westaway, R., and Jackson, J., 1987. The earthquake of 1980 November 23 in Campania-Basilicata (southern Italy), Geophys. J. R. astr. Soc., 90, 375-443.
Zahradnik, J. and F. Hron, 1987. Seismic ground motion of sedimentary valleys - example La Molina, Lima, Peru. J. Geophys., 62, 31-37.

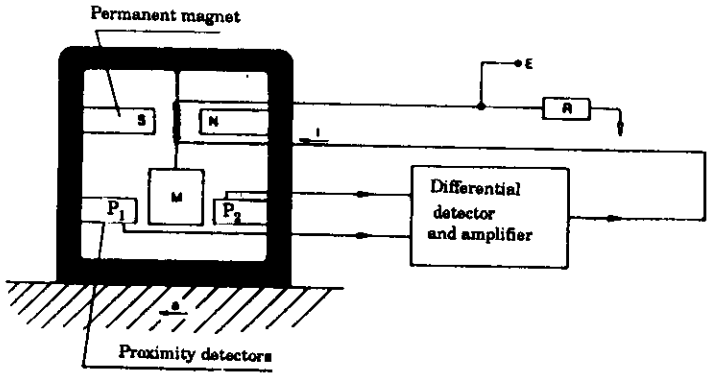

Fig. 2-1. Schematic representation of a force-balance accelerometer (after Roca, 1989).

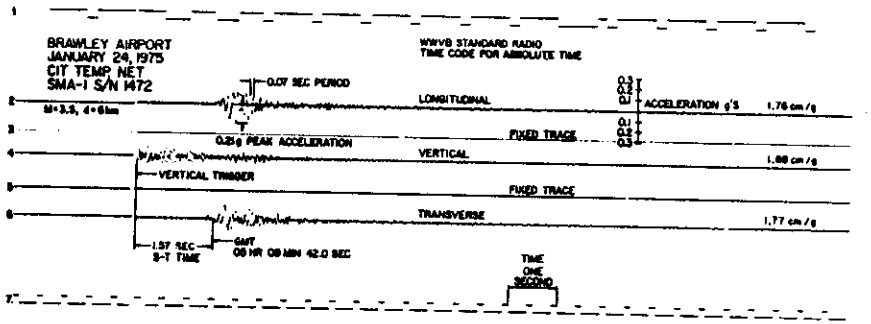

Fig. 2-2. Typical most complete form of analog accelerogram (Hudson, 1979).

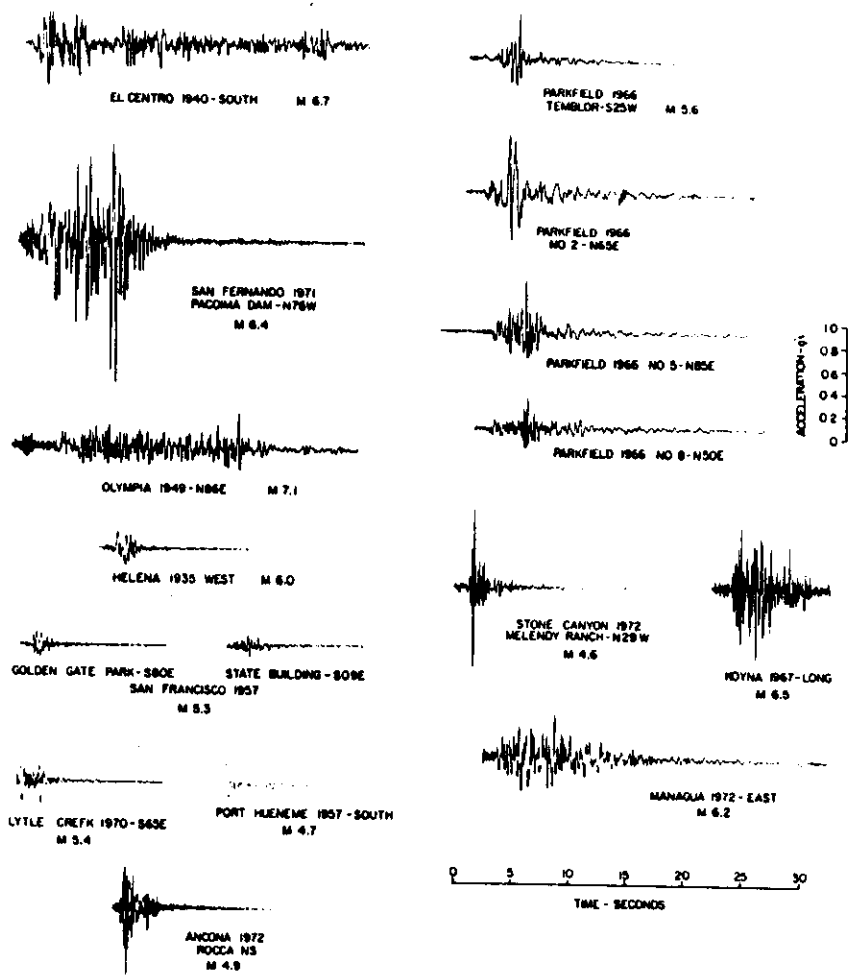

Fig. 2-3. A collection of representative accelerograms (Hudson, 1979).

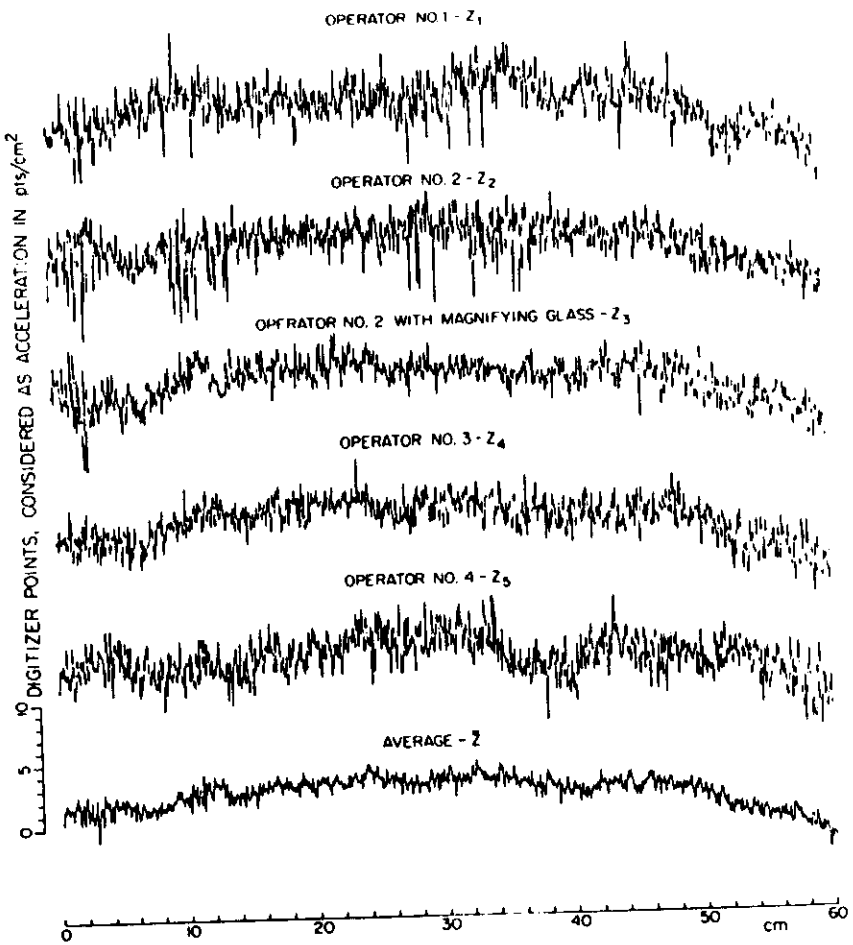

Fig. 2-4. Digitization of a straight line: random errors of different operators (Hudson, 1979).

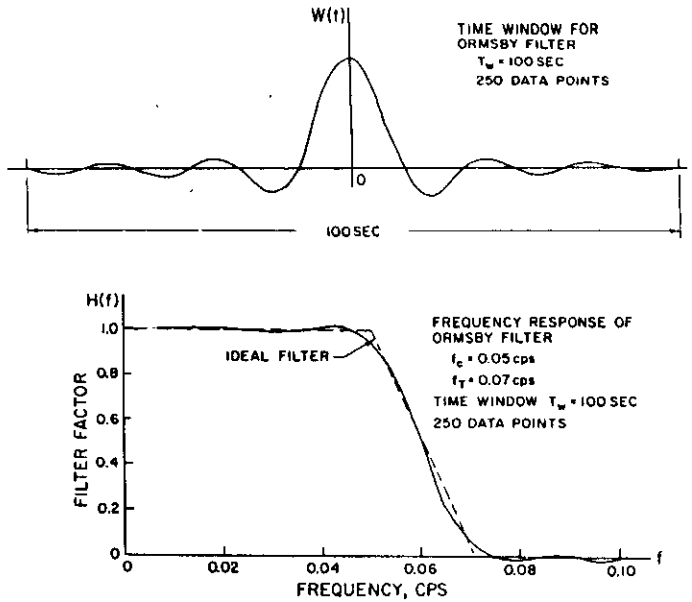

Fig. 2-5. "Ormsby" filter used in standard earthquake data processing (Hudson, 1979).

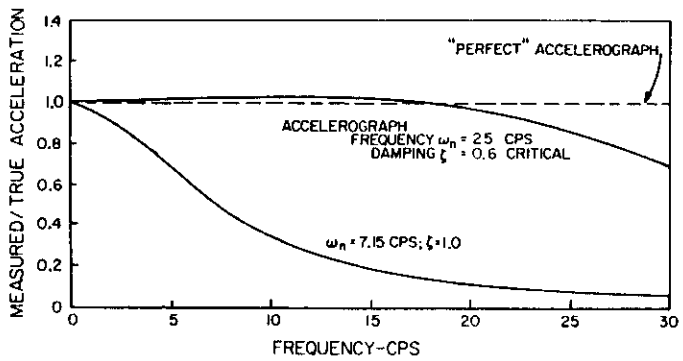

Fig. 2-6. Accelerometer transducers commonly used in strong motion accelerographs have natural frequencies of about 25 Hz and damping of about 60% of critical. Such transducers give a reasonably acurate representation of ground acceleration over the frequency range 0 to 20 Hz. Above about 20 Hz the transducer response drops off with frequency.

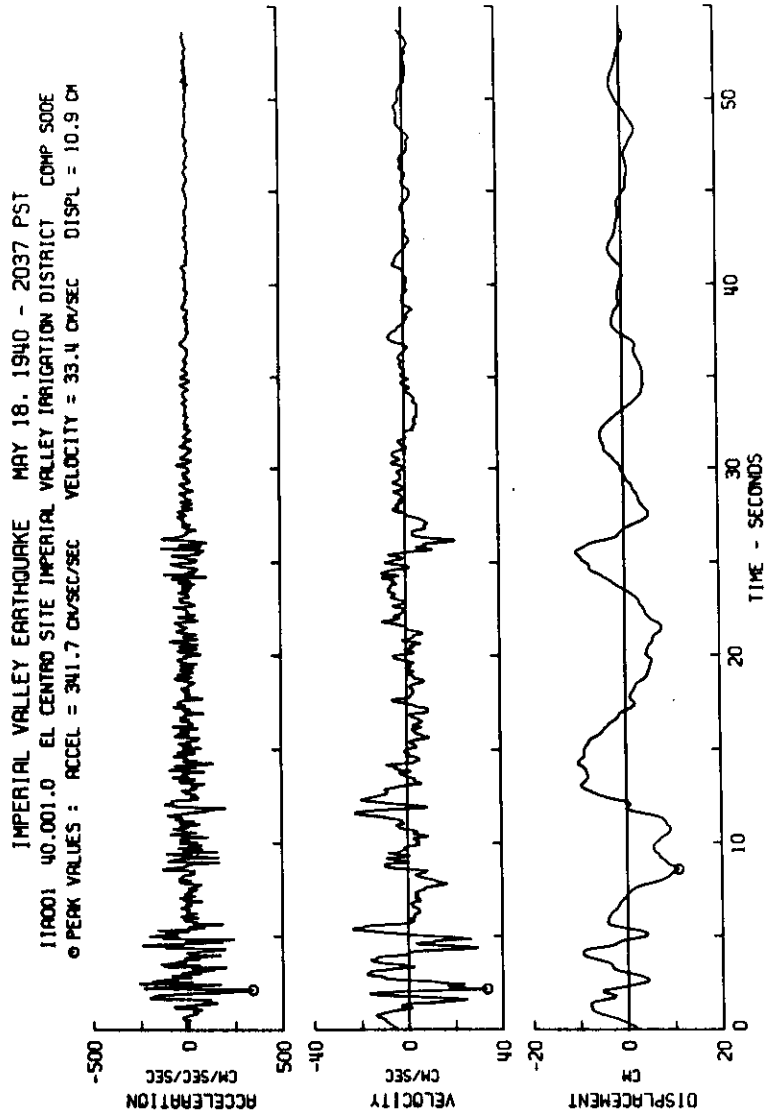

Fig. 2-7. An example of double integration of accelerograms.

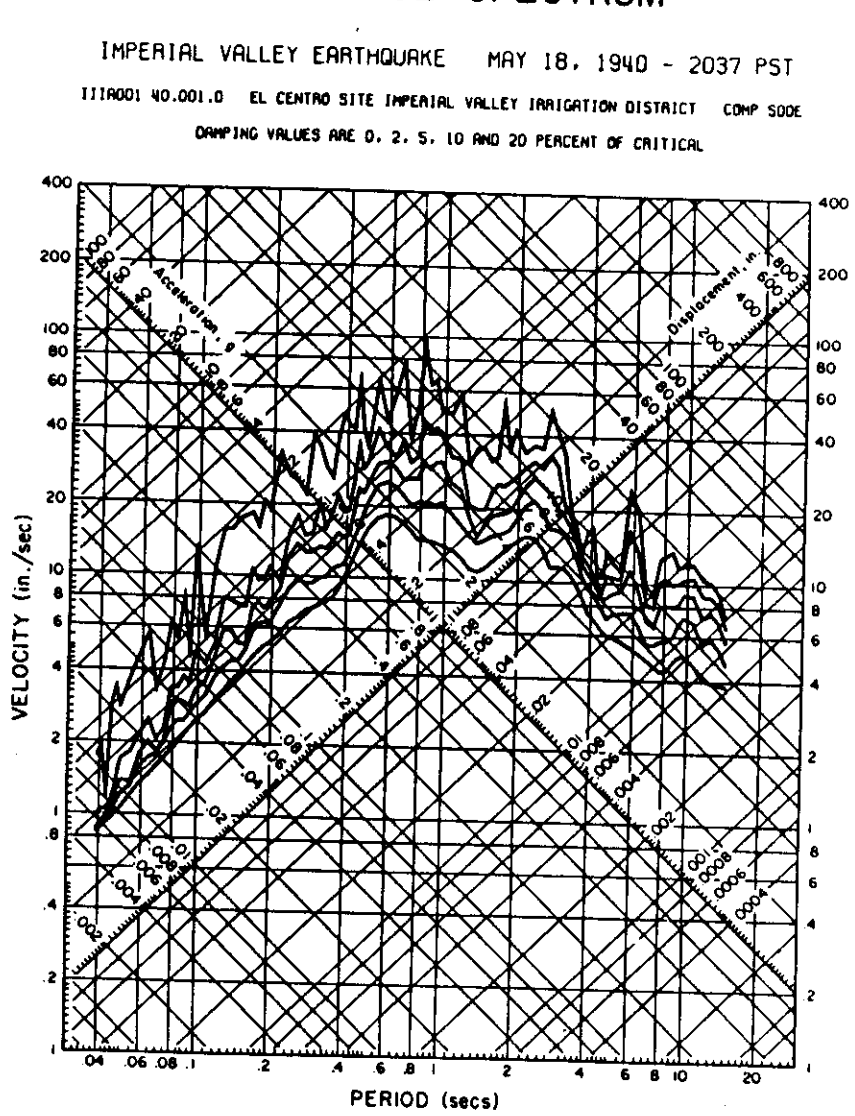

Fig. 2-8. A common form of the response spectrum is the so-called tripartite or four-way logarithmic plot from which the displacement, pseudovelocity and pseudoacceleration spectra can be simultaneously read.

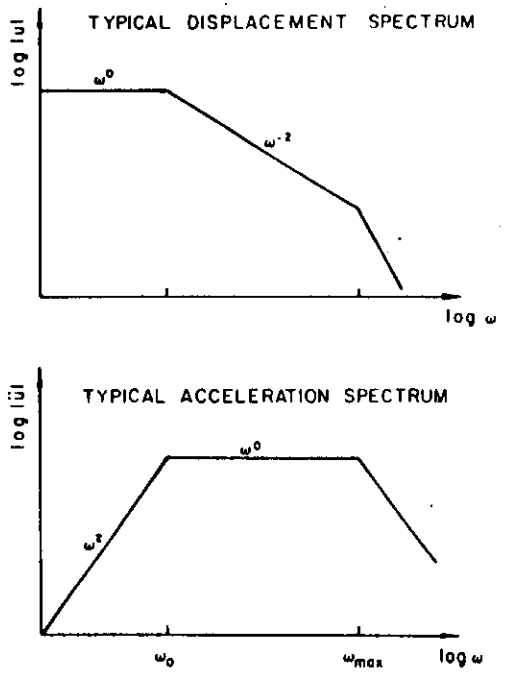

Fig. 3-1. a) Most common form (Brune, 1970) of the displacement *earthquake source spectrum*. b) The acceleration spectrum has a "plateau" between the corner frequency and a frequency called f_{max} (Hanks, 1982).

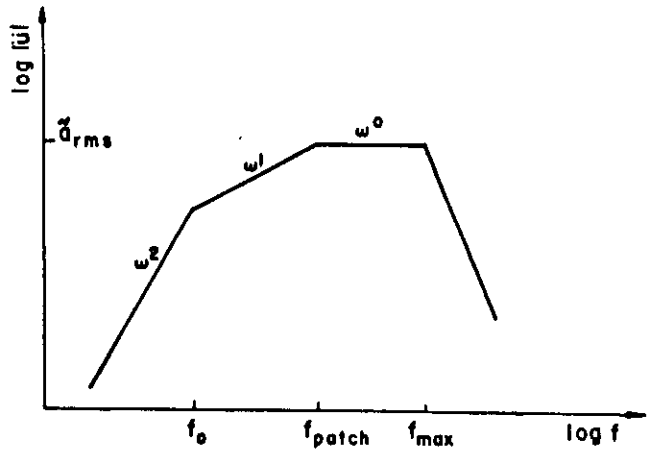

Fig. 3-2. One possible spectrum shows an ω^{-1} envelope before the plateau. The intermediate frequency is called f_{patch} by Papageorgiou and Aki (1983) and reflects the existence of coherent zones with lengths proportional to $(f_{patch})^{-1}$.

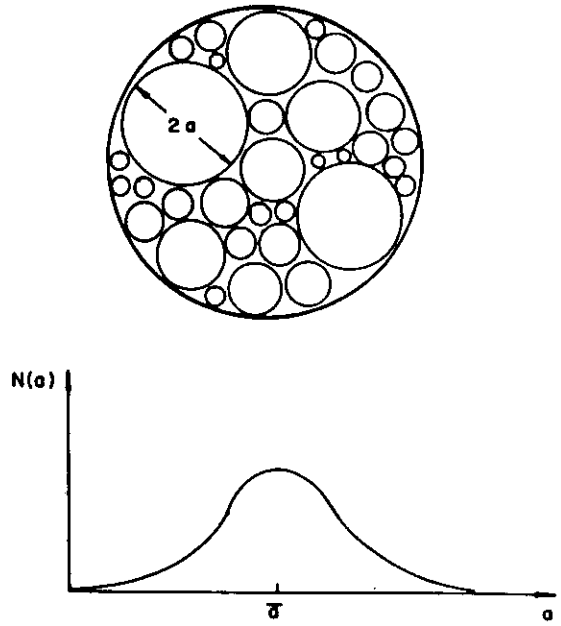

Fig. 3-3. f_{patch} is probably inversely proportional to the mean radius of the active subfaults which radiate on the surface of the fault (after Madariaga, 1989).

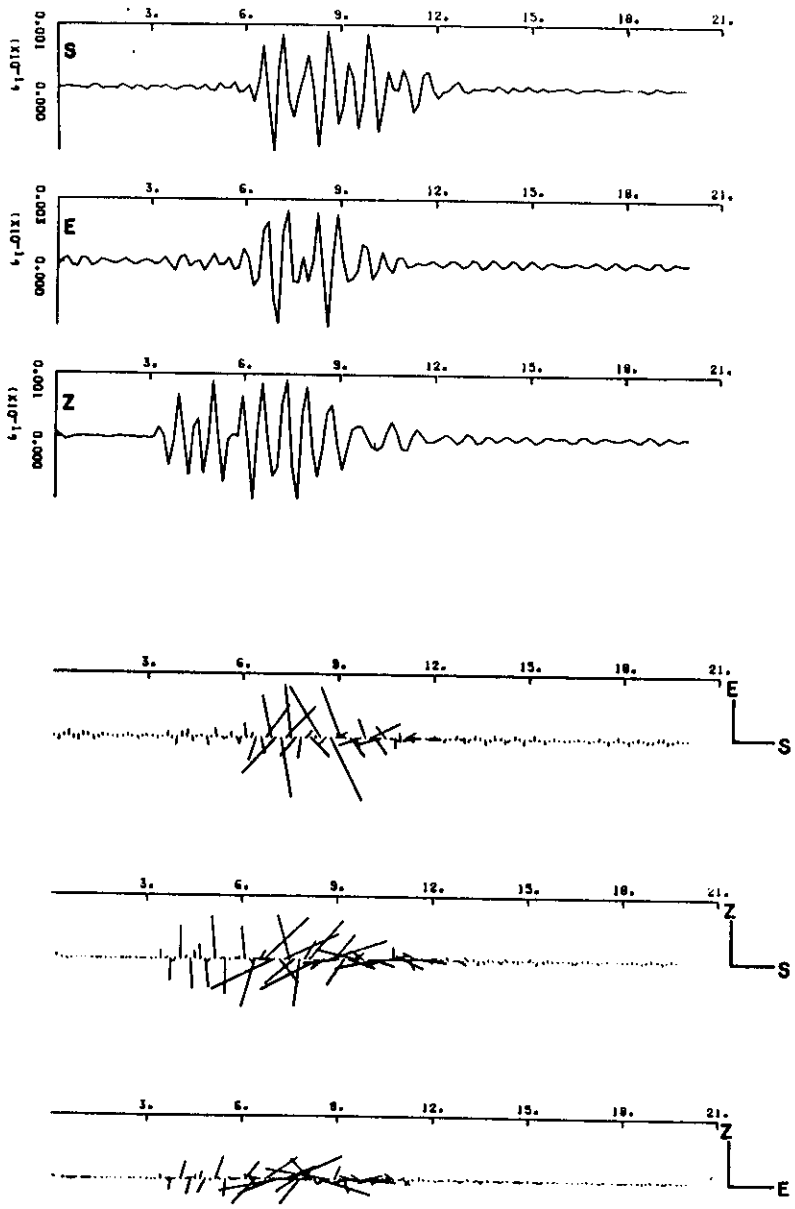

Fig. 4-1. Example of complete synthetics and polarizations for a shallow source. A low-velocity upper layer in the used structural model generates strong multiples and converted phases, whose incoherent arivals make the polarization variable (Zollo and Bernard, 1989).

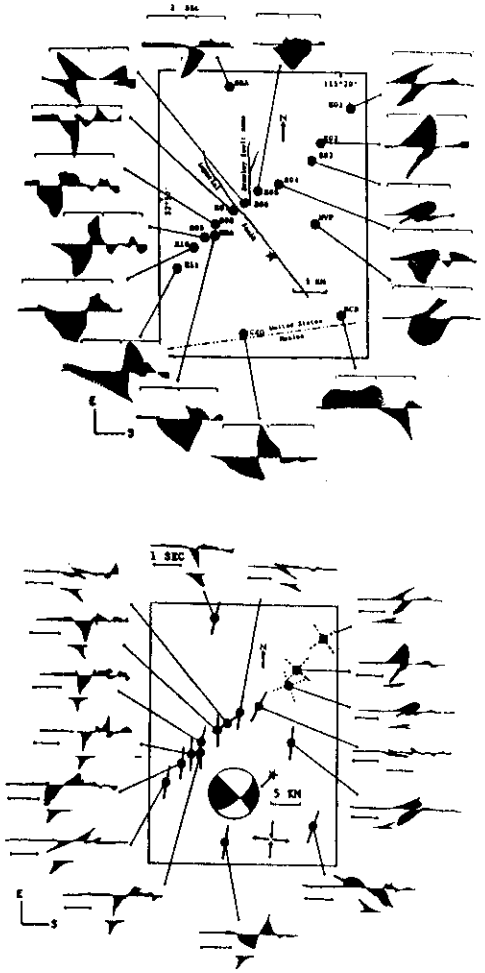

Fig. 4-2. Horizontal polarization vector for S velocity waveforms in the case of the October 15, 1979, 23:19 Imperial Valley, California, earthquake: a) uncorrected, b) corrected for anisotropy After the polarization correction the retrieved source mechanism is much simpler (Zollo and Bernard, 1989).

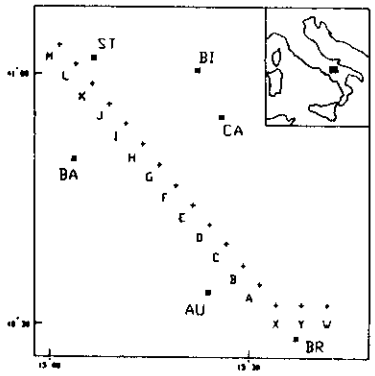

Fig. 5-2. Map of the Irpinia earthquake epicentral area. Crosses indicate the epicentres used in the construction of the synthetic signals. The six considered stations atre: Auletta (AU), Bagnoli Irpino (BA), Bisaccia (BI), Brienza (BR), Calitri (CA) and Sturno (ST).

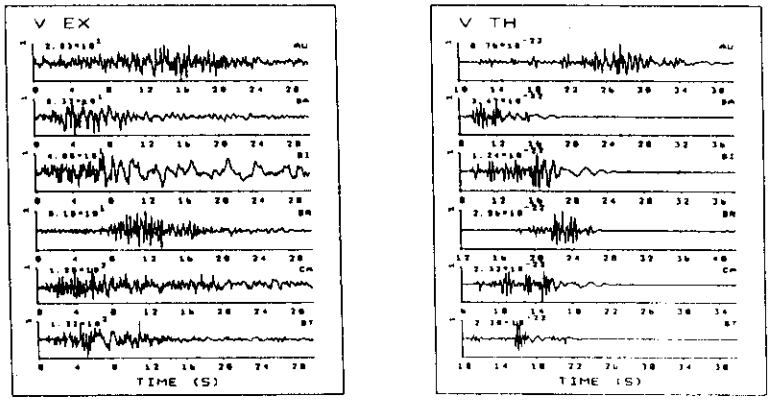

Fig. 5-1. Observed vertical accelerations (first 30 s) at the six considered stations for the Irpinia, Italy, 1980 earthquake.

Fig. 5-3. Synthetic accelerations, the final result of the trial-and-error procedure (see text), obtained superimposing the effect of 12 point sources see also (Figs. 5-4, 5-5).

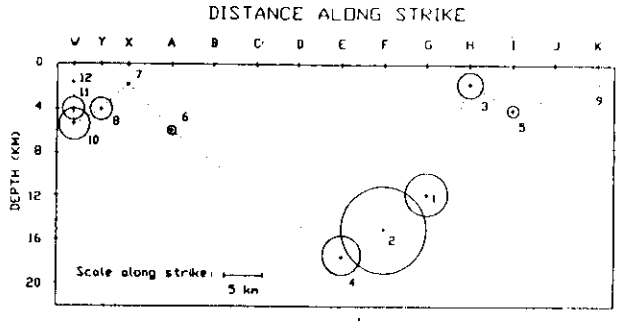

Fig. 5-4. A vertical section of the retrieved source model (point sources used in the construction of the synthetic accelerations of Fig. 5-3).

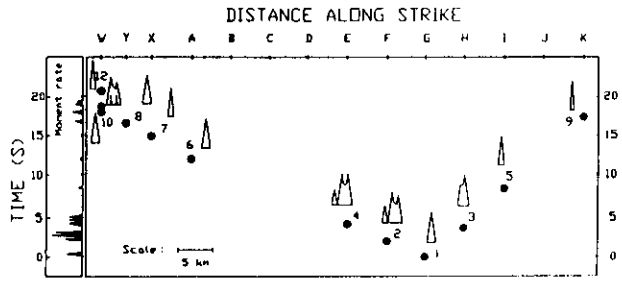

Fig. 5-5. Space-time evolution of the rupturing process.

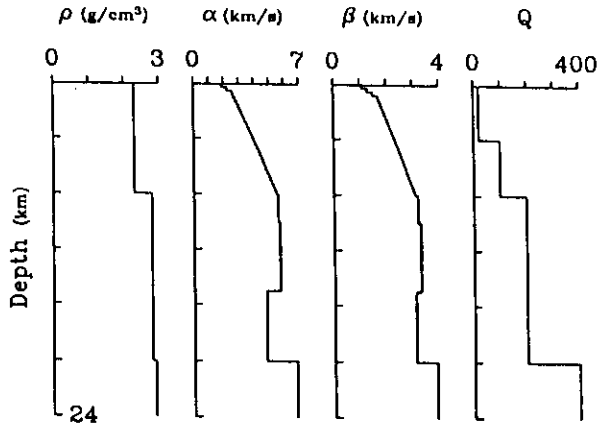

Fig. 5-6. Structural model of the Irpinia area used to compute the synthetics.

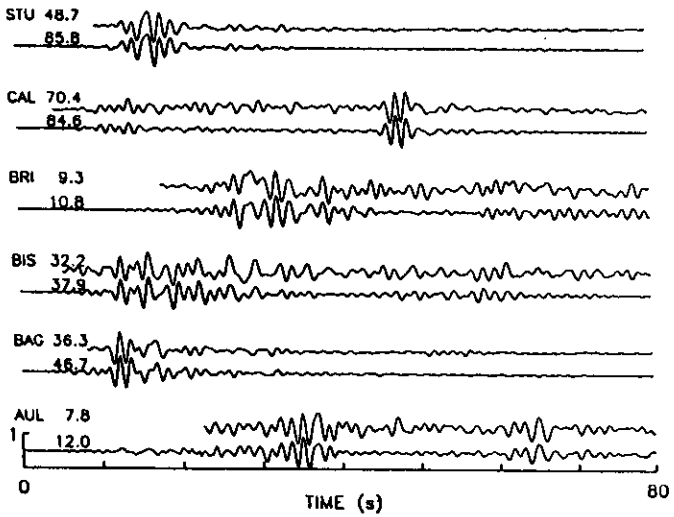

Fig. 5-7. Synthetic accelerograms (lower traces) resulting from the inversion and observed ones (upper traces). They are shown normalized to their maximum amplitude (expressed in cm/s²).

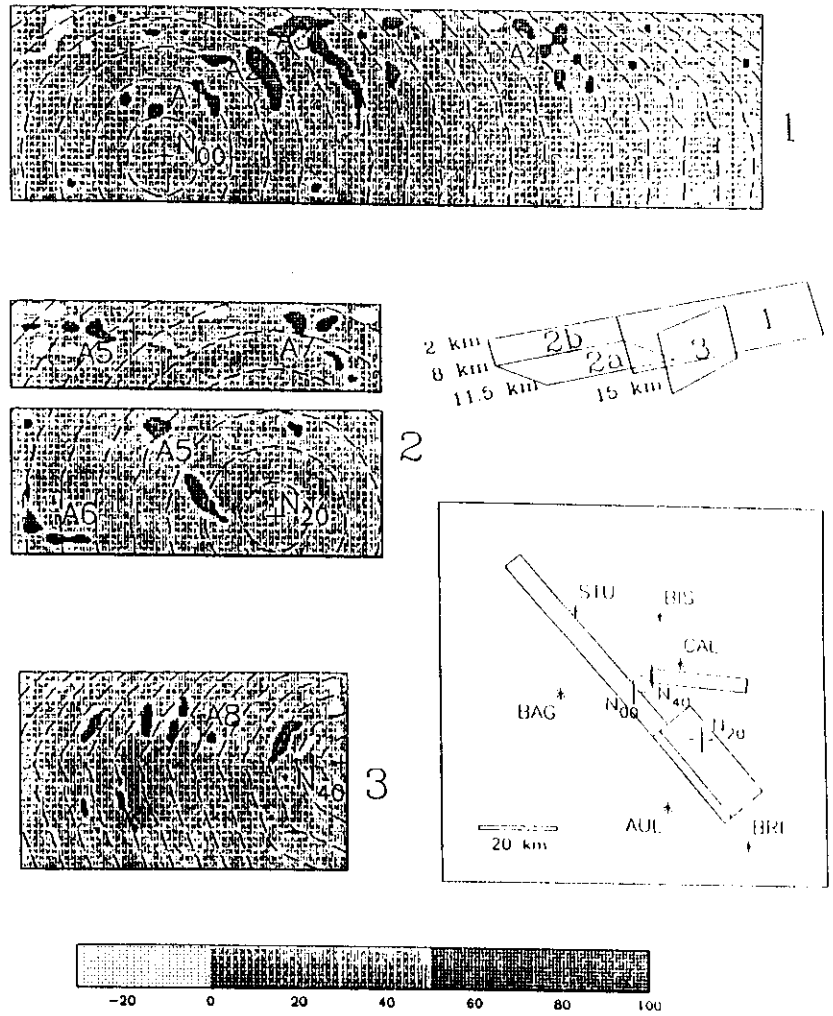

Fig. 5-8. Distribution of moment release along the faults. The moment is normalized to 100 by the maximum estimated value. Dashed lines represent the rupture front at 1 s intervals. The spatial orientation of the faults is shown on the right. (+) nucleation points - (*) stations.

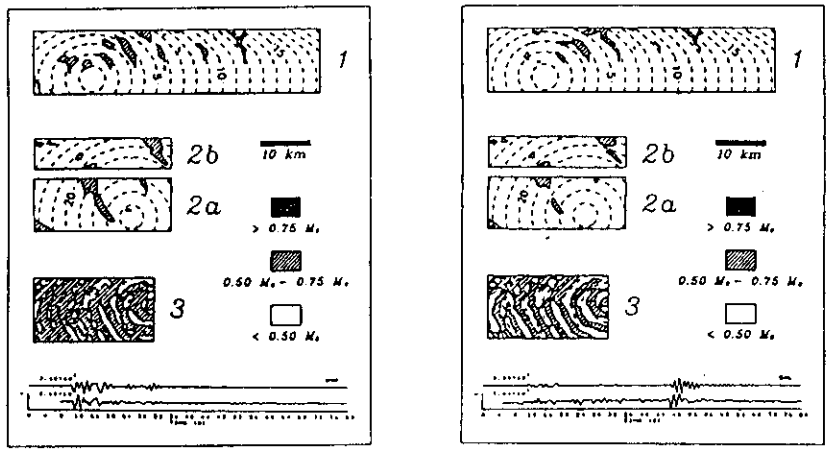

Fig. 5-9. Estimates of strong ground motion in absence of records (see text): a) Bagnoli, b) Calitri.

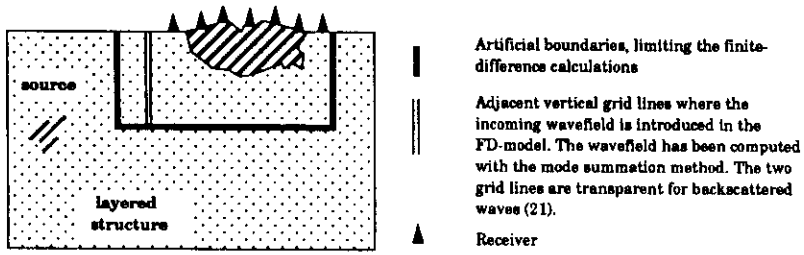

Fig. 5-10. Geometry of the problem. The model is divided into two regions, the 1-D layered structure, where the source is located, and the region containing the 2-D heterogeneities.

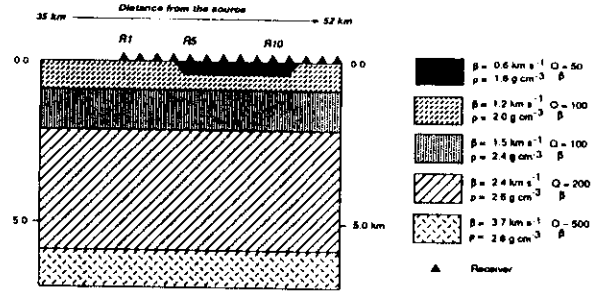

Fig. 5-11. Simple model consisting of a layered structure with only three layers over a halfspace and an alluvial valley. It has been assumed that Q_α=2.5 Q_β and $\alpha = \sqrt{3} \cdot \beta$.

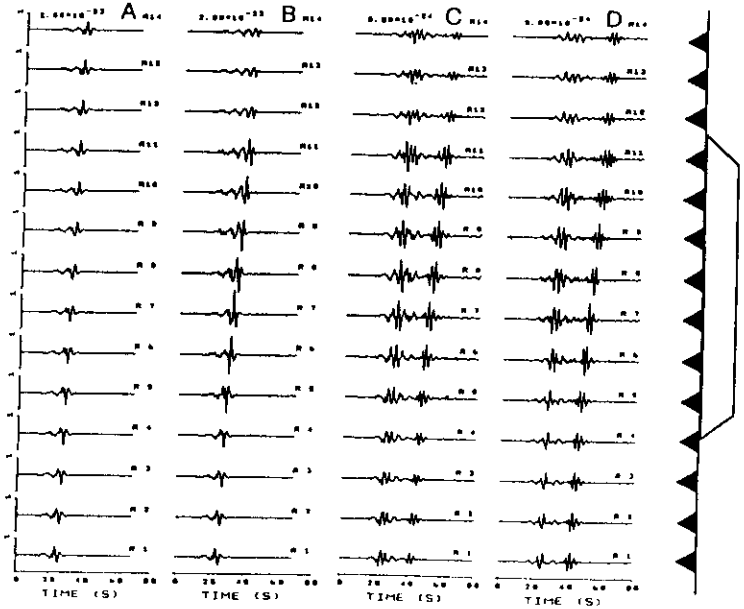

Fig. 5-12. Displacement time series for SH and P-SV waves at an array of receivers (see Fig. 5-11). A right-lateral strike-slip point source with source duration of 1.5 s, placed on a vertical plane at 1.5 km depth, is considered. All amplitudes correspond to a source with seismic moment of 1 dyn cm. The signals are normalized to the maximum peak displacement of all the receivers, shown in the upper part in units of cm. Four different calculations are shown:
A) SH waves, for the layered structure without the basin
B) SH waves, for the model with an alluvial basin
C) radial component of the P-SV waves, for the model with an alluvial basin
D) vertical component of the P-SV waves, for the model with an alluvial basin
The impedance contrast between the valley and the surrounding layer is chosen

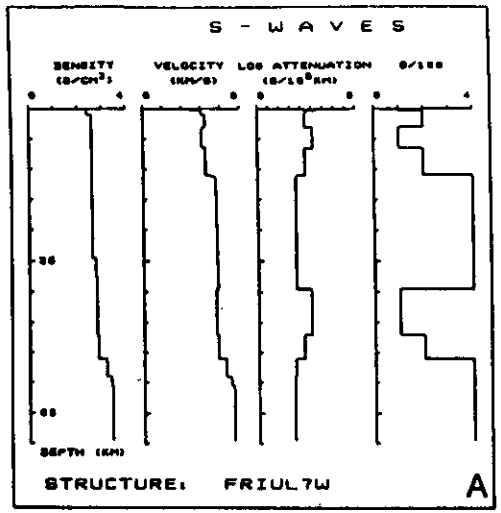

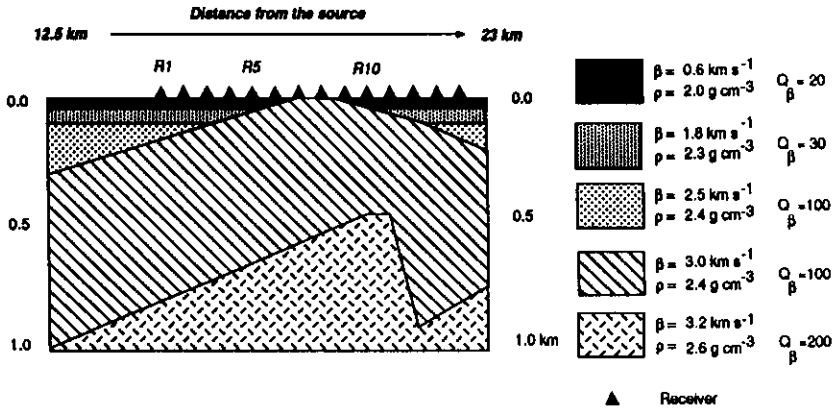

Fig. 5-13. a) 1-D structural model and b) N-S 2-D cross-section of the Friuli central region near Udine. The layered model for the Friuli central region includes two low-velocity zones (Mao and Suhadolc, 1989; 1990). The main features of the N-S cross-section are a series of overthrusts in the southern part and two quarternary basins.

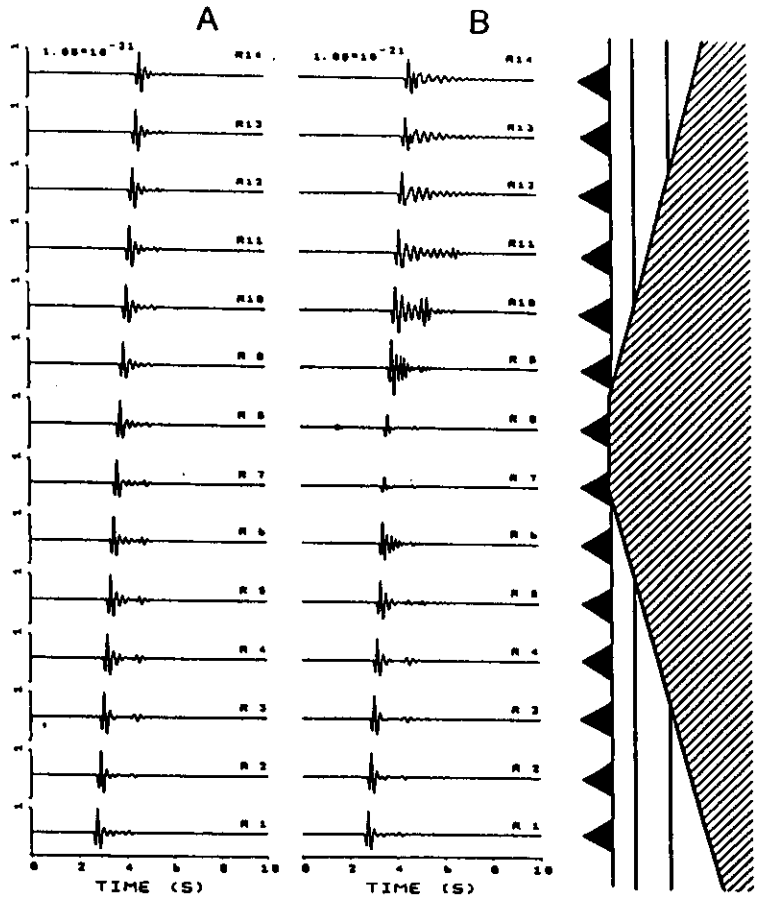

Fig. 5-14. A simulation (upper frequency limit 5 Hz) of the May 6, 1976, Friuli earthquake. Acceleration time series for SH waves at an array of receivers (Fig. 5-12). A point source with source duration of 0.3 s and 7 km depth is considered (strike ϕ=280°, dip δ=30° and rake λ=115°). All amplitudes correspond to a source with seismic moment of 1 dyn cm. The signals are normalized to the maximum peak acceleration of all receivers, shown in the upper part in units of cm/s^2. Two calculations are shown: A) for the layered structure; B) for the laterally heterogeneous structure.